EVALUATION OF FLOW FIELDS IN WETLANDS USING PHYSICAL MODELS

FINAL REPORT

Department of Civil and Environmental Engineering
Department of Mechanical and Aerospace Engineering
Arizona State University
Tempe, Arizona

Agreement Number: 98-FC-81-0051
Desalination Research and Development Program Report No. 49

May 2002

U.S. DEPARTMENT OF THE INTERIOR
Bureau of Reclamation
Technical Service Center
Water Treatment Engineering and Research Group
Denver, CO

EVALUATION OF FLOW FIELDS IN WETLANDS USING PHYSICAL MODELS

FINAL REPORT

Peter Fox - Department of Civil and Environmental Engineering
H.J.S. Fernando, Rudolpho V. Rodriguez, Teresa Serra, Micheal Arzabe -
Department of Mechanical and Aerospace Engineering
Arizona State University
Tempe, Arizona

Agreement Number: 98-FC-81-0051
Desalination Research and Development Program Report No. 49

May 2002

U.S. DEPARTMENT OF THE INTERIOR
Bureau of Reclamation
Technical Service Center
Water Treatment Engineering and Research Group
Denver, CO

REPORT DOCUMENTATION PAGE

Form Approved
OMB No. 0704-0188

1. AGENCY USE ONLY *(Leave Blank)*	2. REPORT DATE	3. REPORT TYPE AND DATES COVERED
	May 2002	Final

4. TITLE AND SUBTITLE
Evaluation of Flow Fields in Wetlands Using Physical Models

5. FUNDING NUMBERS

6. AUTHOR (S)
Peter Fox, H.J.S. Fernando, Rudolpho V. Rodriguez, Teresa Serra, Micheal Arzabe

7. PERFORMING ORGANIZATION NAME(S) AND ADDRESS(ES)
Arizona State University
Department of Mechanical and Aerospace Engineering
Department of Civil and Environmental Engineering
Tempe, AZ

8. PERFORMING ORGANIZATION REPORT NUMBER
DRDP Report No. 49

9. SPONSORING/MONITORING AGENCY NAME(S) AND ADDRESS(ES)
Bureau of Reclamation
Denver Federal Center
PO Box 25007
Denver CO 80225-0007

10. SPONSORING/MONITORING AGENCY REPORT NUMBER

11. SUPPLEMENTARY NOTES

12a. DISTRIBUTION/AVAILABILITY STATEMENT
Available from the National Technical Information Service, Operations Division, 5285 Port Royal Road, Springfield, VA 22161

12b. DISTRIBUTION CODE

13. ABSTRACT *(Maximum 200 words)*
To evaluate fluid flow in different wetland designs under controlled laboratory conditions to determine relationships between wetland design parameters and flow characteristics. Compared laboratory results to field-scale systems using tracer studies at the Tres Rios Wetlands Demonstration Project in Phoenix, Arizona.

14. SUBJECT TERMS—wetland design parameters, field-scale tracer studies

15. NUMBER OF PAGES
45

16. PRICE CODE

17. SECURITY CLASSIFICATION of REPORT	18. SECURITY CLASSIFICATION OF THIS PAGE	19. SECURITY CLASSIFICATION OF ABSTRACT	20. LIMITATION OF ABSTRACT
UL	UL	UL	UL

NSN 7540-01-280-5500 **Standard Form 298 (Rev. 2-89)**

Prescribed by ANSI Std. 239-18298-1

U.S. Department of the Interior
Mission Statement

The mission of the Department of the Interior is to protect and provide access to our Nation's natural and cultural heritage and honor our trust responsibilities to tribes.

Bureau of Reclamation
Mission Statement

The mission of the Bureau of Reclamation is to manage, develop, and protect water and related resources in an environmentally and economically sound manner in the interest of the American public.

Acknowledgements

The author would like to thank the Desalination Research and Development Program, Bureau of Reclamation, and the City of Phoenix for sponsoring this research. The authors would like to thank Bob Jurenka of the Bureau of Reclamation and Aimee Conroy, Paul Kinshella, and Roland Wass of the City of Phoenix for their time and efforts to complete this project.

In addition, the authors thank all the students who helped with this project at the Center for Environmental Fluid Dynamics and the National Center for Sustainable Water Supply at Arizona State University.

Disclaimer

Information contained in this report regarding commercial products or firms was supplied by those firms. It may not be used for advertising or promotional purposes and is not to be construed as an endorsement of any product or firm by the Bureau of Reclamation.

The information contained in this report was developed for the Bureau of Reclamation; no warranty as to the accuracy, usefulness, or completeness is expressed or implied.

TABLE OF CONTENTS

Tables

Figures

EXECUTIVE SUMMARY

The main objective of this project was to evaluate fluid flow in different wetland designs under controlled laboratory conditions to determine the relationships between wetland design parameters and flow characteristics. Wetlands are a potential component of desalination systems. Wetlands may be used to grow salt-tolerant plants, thereby aiding in the disposal of brine solutions. Wetlands can also be used to remove inorganic ions from saline wastewaters. Laboratory results were compared to field-scale systems where extensive tracer studies were performed at the Tres Rios Wetlands Demonstration Project in Phoenix, Arizona. The Tres Rios Wetlands Demonstration Project was funded in part by the U.S. Bureau of Reclamation and contained 16 different wetlands with seven different open-water deep zone configurations. Four of the wetlands with different open-water deep zone configurations were used in this study. Field-scale tracer studies used influent and effluent data to determine the impacts of wetland design parameters on residence times and dispersion. However, field scale tracer studies do not provide information on how wetland design parameters affect internal mixing in different sections of the wetlands. Controlled laboratory experiments were used to provide insight into micro-scale fluid flow issues, and the results were compared to macroscopic observations made from full-scale tracer tests.

A physical model of a wetland to assess flow fields as a function of wetland design parameters was constructed at a scale of 20:1. The model was scaled and tested to simulate field conditions. The model was capable of testing different flow rates, emergent zone to deep zone transitional slopes and different emergent or deep zone lengths. Flow patterns were visualized using particle-tracking velocimetry, which provided information on salient flow structures. Simultaneously with particle-tracking, the technique of laser-induced fluorescence was used to observe and quantify the mixing in various zones of the flow. A series of tests were done under conditions scaled for comparison to field-scale tracer studies. Several series of tests were performed to systematically evaluate the impacts of wetland design parameters on flow fields.

The results demonstrated that establishment of recirculation in deep zones was a function of both the water depth and the slope of the transition between the vegetative zone and the deep zone. The deep zone width and the deep zone length were not critical to establish recirculation. A relationship was developed to determine requirements for transitional slope and water depth to establish recirculation. All field-scale testing was done under conditions where recirculation should have been established. Consequently, analysis of field-scale tracer tests yielded a number of mixed tanks that were always equal to or greater than the number of deep zones. From macroscopic analysis, each deep zone appeared to behave as a completely mixed system consistent with established recirculation.

The lateral diffusivity created by flow through a vegetated zone does not appear to influence longitudinal dispersion in basin H1 where five deep zones were present. The longitudinal dispersion for basin H1 was independent of the presence of vegetation.

Other basins contained longer vegetated zones, and higher dispersion numbers were observed in these basins. This might imply that lateral diffusivity becomes more important as the vegetative zone length increases and the number of deep zones decreases. The presence or absence of vegetation did not affect water quality improvement in basins H1 and H2. The main effect of flow fields on the performance of wetlands systems is the establishment of recirculation in deep zones. This redistributes the flow prior to entrance into a subsequent vegetative zone and maintains residence times in the systems that are close to theoretical.

BACKGROUND

Constructed wetlands have been used for a wide variety of wastewater treatment and reclamation purposes. Applications have included the treatment of industrial wastewaters, agricultural wastewaters, and municipal wastewaters. Salt-tolerant plants may be used to treat saline wastewaters. Changes in pH and ion content during wetlands treatment can be used to remove ions and reduce salinity. The benefits of reuse and reclamation of wastewaters with constructed wetlands are not limited to improvements in water quality. Enhancement or creation of wildlife habitat is often a major benefit in terms of public perception. The EPA has a goal of creating 25,000 acres of wetlands per year to help mitigate wetland losses throughout the United States of America. Constructed wetlands are an excellent method of reclaiming wastewaters and creating wetland habitat.

Several different methods for utilizing constructed wetlands in desalination processes have been tested and proposed for many different applications. The disposal of brine solutions in saline wetlands has been proposed as a method for brine reclamation (Crothers-Christie Moon, 1994). Saline wastewater reuse in Jabail, Saudi Arabia, has been enhanced through the use of constructed wetlands (Al-A'ama and Nakhla, 1995). The brine solutions can be used to grow salt-tolerant wetland plants that have beneficial uses. Removal of contaminants such as high nitrate concentrations has been demonstrated in saline solutions such as spent regenerant brine from ion-exchange systems (Clifford and Liu, 1993, Yang et al., 1995). The actual removal of specific dissolved ion components of saline industrial wastewaters has also been documented. Constructed wetlands have been used to treat mine tailings and industrial landfill leachates (Martier et al., 1995). Littlejohn and Chang (1984) reported combined desulfurization and denitrification. The potential of constructed wetlands for beneficial reuse of saline solutions by either brine disposal or for the removal of specific constituents has not been fully exploited.

The major mechanisms for contaminant removal in wetland systems depend on transport of dissolved substances to sediments, roots, and plant surfaces. Several studies have been done to characterize removal as a function of hydraulic parameters. The effects of substrate type, surface water depth, and flow rate on manganese removal in simulated wetland systems were reported by Stark et al. (1996). Nitrate removal in riparian wetland soils was studied as a function of flow rate, temperature, nitrate concentration, and soil

depth by Willem et al. (1997). The degradation of phenanthrene was related to hydraulic characteristics in a constructed wetlands by Machate et al. (1997). Water quality monitoring was performed at the Tres Rios Demonstration Wetlands site since 1995 (Stiles et al., 2001) and Status Report to the 1998 Research Plan for the Tres Rios Demonstration Constructed Wetland Project (Wass et al., 2001). These studies provide insight into the relationship between constructed wetland hydraulics and contaminant removal; however, there is no information on internal mixing and actual flow fields within the systems studied. These studies did not report on the impacts of the areal extent of deep zones and vegetated zones on system performance either.

One of the major reasons cited for failure of constructed wetland systems is poor hydraulic characteristics (Mitsch and Gosselink, 1993). Variable plant densities often lead to short-circuiting through zones with less plant growth. Limited contact of water with sediments, roots, and plants results in poor treatment performance. Proposed constructed wetland design options to overcome problems with short-circuiting include the use of different plant species, kidney-shaped basins, and alternating deep zones with emergent zones.

The use of deep zones alternating with vegetative zones is one of the most common methods of improving the hydraulic characteristics of constructed wetlands (Kadlec and Knight, 1996). Deep zones are believed to improve hydraulic performance by allowing water to mix after flowing through a vegetative zone. The water enters the next vegetative zone with an evenly distributed flow path even if the water has short-circuited through the previous vegetative zone. Deep zones are designed deep enough to prevent the growth of emergent vegetation. Deep zones are also believed to enhance anoxic removal mechanisms such as denitrification since transport of oxygen to the bottom of deep zones is limited. Finally, deep zones enhance wildlife habitat by creating a more complete ecosystem in the wetlands capable of sustaining aquatic birds and other species requiring open water.

A systematic evaluation of constructed wetlands to determine the impacts of different deep zone and vegetative zone configurations was one of the purposes of building the Tres Rios Demonstration Wetlands. A tracer-testing program was developed to perform field-scale tracer tests on all 16 of the wetlands that comprise the Tres Rios Demonstration Wetlands. The tracer tests were performed by adding pulses of bromide at the influent of the constructed wetlands and analyzing the effluent bromide concentrations. The data is analyzed to determine average detention times, residence time distributions, and dispersion. Results of the field-scale tracer tests must be corrected for the effects of evaporation, precipitation, and infiltration to properly characterize basin hydraulics. This classical approach to performing tracer tests will not demonstrate how different deep zone and vegetative zone configurations affect internal mixing and flow fields. The classical approach provides insight into the macroscopic flow characteristics of a system.

The detention time and flow field within each deep zone and vegetative zone can be characterized through the use of physical models to simulate the field-scale systems. At

the Tres Rios Demonstration Wetlands, the four largest wetlands all have 20 percent open water area and 80 percent vegetation. Depending on the water depth, the volume of water in the deep zones can be greater than 50 percent of the total wetland volume and the theoretical detention time in the deep zones is also greater than 50 percent of the total theoretical detention time. Therefore, determining the actual distribution of detention times and flow fields in both deep zones and vegetative zones is critical to determining the optimal design for constructed wetlands and how contaminant removal occurs as a function of design parameters. Physical models provide insight into micro-scale flow characteristics in the deep zones and shallow zones and therefore, provide insight into full-scale tracer studies.

Environmental factors and water mass balance effects complicate interpretation of field-scale tracer test results. Data must be corrected for evapotranspiration and precipitation, which impact the water mass balance. Infiltration of water into the ground will result in the loss of water and associated tracer. Temperature changes and wind can also affect tracer results in unpredictable patterns. The use of physical models to simulate constructed wetlands will allow for an analysis of flow fields under controlled conditions where the impacts of environmental factors and water mass balance changes will be minimized.

During this study, a physical model was used to study the flow distribution, detention times, and vertical mixing characteristics of constructed wetlands. These characteristics were determined as functions of governing parameters, namely, the depth and shape of the deep zone, volumetric flow rate, morphology and density of the vegetated zones (measured as a fraction of the emergent plant area in the vegetated zone). Use of physical models and dynamic similarity techniques to study hydraulic phenomena is very common and effective (Brutsworth 1983), and this work should help determine favorable parameter ranges for design and operation of artificial wetlands. To our knowledge, wetland configurations with a vegetated zone with incident uniform flow emanating from a deep trench have not been modeled before, and this work provides new information on flow phenomena and parameterizations pertinent to constructed wetlands.

TECHNICAL APPROACH

FIELD SITE SUMMARY DESCRIPTION

The Tres Rios Demonstration Wetlands consist of three adjacent sets of constructed wetland basins. These sets of constructed wetlands are referred to as the Cobble site, the Hayfield site, and the Research Cells (figures 1 and 2). The Cobble site contains two parallel constructed wetlands of identical area (basins C1 and C2). The Hayfield site contains two parallel constructed wetlands of identical area (basins H1 and H2). All four basins at the Hayfield and Cobble sites are configured with an areal distribution of 20 percent deep zones and 80 percent vegetated zones. Both basins C1 and C2 at the Cobble site have three deep zones. Unlike all the other basins at the Tres Rios Demonstration site, basin C1 is not lined, and the majority of water entering the basin infiltrates into the

Figure 1. - Aerial photograph of the Tres Rios Demonstration Wetlands (taken from the south).

groundwater. At the Hayfield site, basin H1 has five deep zones, while basin H2 has two deep zones. There are 12 research cells (basins R1-R12) which are comprised of three identical sets of four different designs. The four different designs have deep zone areas that range from 11 percent to 35 percent of the total area. A series of tracer tests were initiated in November of 1995. These tests were conducted once in each of the 12 Research Cell basins, four times in basin H1, three times in basin H2 and one time each in basins C1 and C2. This study focuses on the tracer testing in basins H1, H2 and C2. Results from tracer tests completed in the research cells are questionable since the mass recovery of tracer was less than 50 percent. Also, the third set of tests done in H1 and H2 had autosampler failure resulting in an incomplete data set. The flow characteristics in basin C1 are very different since the majority of water infiltrates into the ground.

Figure 2. - Overhead aerial photograph of the Tres Rios Demonstration Wetlands.

WETLAND BASIN DESCRIPTION

Tracer testing conducted at the Hayfield Riparian site was designed to assess differences in hydraulic retention time (HRT) and mixing characteristics with respect to the configuration of open-water deep zones within a constructed treatment wetland. One set of tests was completed with minimal vegetative coverage. While not originally anticipated, this test provides a comparison between a system with dense vegetation and a system with minimal vegetation.

The Tres Rios Demonstration Wetland sites used for the majority of tracer testing were the Hayfield Riparian Wetland basins H1 and H2 (figure 1). Each basin is approximately 3 acres in wetted surface area with 20 percent of the total as open-water deep zones. Basin H1 has its 20 percent open water configured into five narrow (top width = 30 feet), sinusoidal deep zones placed perpendicular to the main flow path and spaced at roughly 88-foot intervals. Basin H2, on the other hand, has its 20 percent open water configured into two wide (top width = 75 feet) internal deep zones. Remaining basin morphology is presented in table 1.

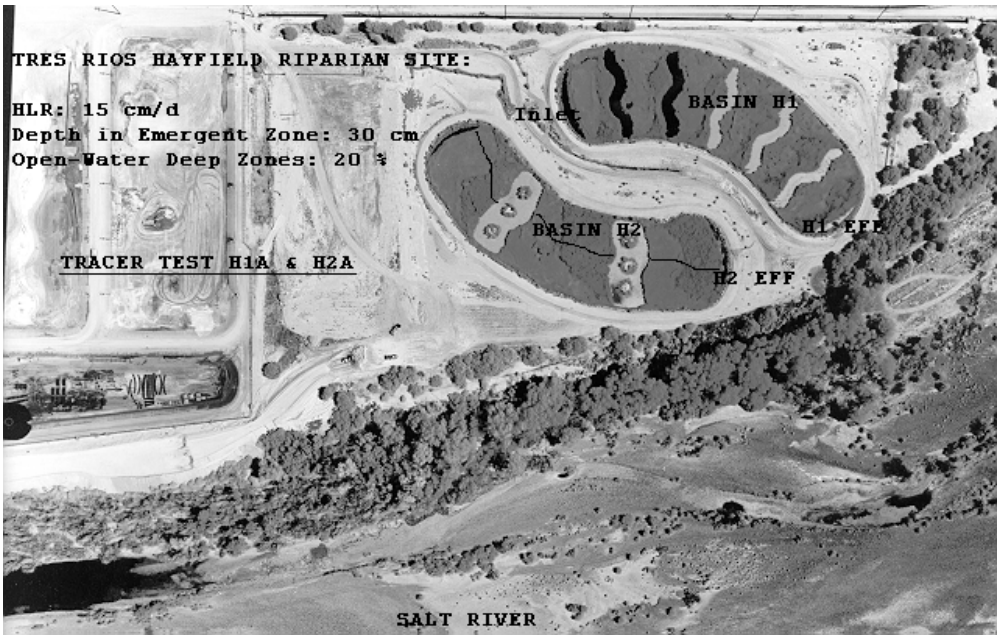

Figure 3. – Tres Rios Demonstration Wetlands, Hayfield Riparian site basins H1 and H2.

Table 1. - Hayfield site basin geometry

Parameter	H1	H2
Length	228 m (748 ft)	228 m (748 ft)
Width	60 m (200 ft)	60 m (200 ft)
Aspect ratios	3.8:1	3.8:1
Exterior berm top width	3.7 m (12 ft)	3.7 m (12 ft)
Exterior berm side slope	3:1	3:1
Elevation gradient inlet to outlet	0.15 m (0.5 ft)	0.15 m (0.5 ft)
Basin slope	0.0007 ft/ft	0.0007 ft/ft
Inlet deep zone top width	8.5 m (28 ft)	8.5 m (28 ft)
Interior deep zone top width	9 m (30 ft)	23 m (75 ft)
Deep zone spacing	27 m (88 ft)	55 m 9180 ft)
Deep zone depth	1 m (3.3 ft) below cell floor	1 m (3.3 ft) below cell floor
Deep zone side slope	3:1	3:1

Calculated basin volumes for tracer analysis were developed using the basin parameters given in table 1 as a guide, and Bureau of Reclamation (Reclamation) aerial survey data to define discrete areas (individual deep and emergent zones), and individual zone depths obtained by level survey. Results of this endeavor are provided in table 2.

Table 2. – Hayfield site basin volumes

Basin	Emergent area depth	Volume	Reclamation model flight date
H1	1.0 ft (0.3 m)	7,019.2 m^3	4/8/96
H2	1.0 ft (0.3 m)	6,237.7 m^3	4/8/96
H1	1.5 ft (0.46 m)	9,443.2 m^3	8/4/97
H2	1.5 ft (0.46 m)	8,420.4 m^3	8/4/97

Two tests were completed in the Cobble site basins that are each approximately 2.2 acres in wetted surface area. Basin C1 is unlined and has almost 50 percent deep water, while C2 is lined and has roughly 20 percent of its surface area as deep zone. Furthermore, basin C2 has approximately 0.3 acres of islands located in the emergent zone areas. Remaining basin morphology is presented in table 3.

Table 3. – Cobble site basin geometry

Parameter	C1 and C2
Length	275 m (748 ft)
Width	35 m (115 ft)
Aspect ratios	7.9:1
Exterior berm top width	3.7 m (12 ft)
Exterior berm side slope	3:1
Elevation gradient inlet to outlet	0.15 m (0.5 ft)
Basin slope	0.0007 ft/ft
Inlet deep zone top width	10.6 m (35 ft)
Interior deep zone top width	9 m (30 ft) & 25 m (85 ft)
Deep zone spacing	55 m (180 ft)
Deep zone depth	1 m (3.3 ft) below cell floor
Deep zone side slope	3:1

As for the Cobble basins, calculated basin volumes for tracer analysis were developed using the basin parameters given in Table 3 as a guide, and Reclamation aerial survey data to define discrete areas (individual deep and emergent zones), and individual zone depths obtained by level survey. Results of this endeavor are provided in table 4.

Table 4. – Cobble site basin volumes

Basin	Emergent Area Depth	Volume	Reclamation Model Flight Date
C1	1.5 ft (0.46 m)	6,724.0 m^3	1/00
C2	1.5 ft (0.46 m)	4,780.9 m^3	1/00

Details of the tracer analysis results are presented in the "Results and Discussion" section.

PHYSICAL MODEL SUMMARY DESCRIPTION

The flow configuration of a wetland system is complex, and hence analytical prediction of the flow and dispersion is impractical. The use of numerical studies will also be inappropriate for the same reason as the flow involves a range of scales (varying from the basin scale to the energy dissipating Kolmogorov scale of turbulence), of which

Resolution demands unreasonable computing resources. As such, the best tool for analysis of the flow configuration of interest will be the use of hydraulic modeling in conjunction with simple theoretical (phenomological) developments. A physical model was constructed to simulate flow in the Hayfield basins to complete hydraulic modeling studies under conditions similar to field-scale conditions.

Summary Description of Laboratory Facility

The physical model of the Hayfield Riparian site was built in a tank of dimensions 12.2 x 0.46 x 0.34 meters. The bottom and sides are made of plexiglas. The top is open, but can be covered with constructed wooden lids. A series of wooden boxes and wedges was built to form a model of the actual basin. Each box represents a vegetated zone, and wedges attached to each end of the box represent the slope connecting the vegetated zone to a deep zone (figures 4(a), 4(b), and 4(c)).

The design dimensions were determined by scaling down the full-scale system by a factor of 20. The design flow rate was set so that the Reynolds numbers, with respect to deep zone depth and vegetation diameter, would match those of the actual constructed wetland. The laboratory facility was equipped with a laser and a high-resolution video camera used for flow analysis.

For particle tracking velocimetry purposes, we placed the origin of the coordinate system at the end of the first shallow zone. This is shown in figure 4(b).

In figure 4(c), we only show the first window length, from x = 0 to 15 cm, and the last window length, from 105 to 115 cm. The other windows are in intermediate positions in the flat part of the deep zone. In this figure, we also show the significance of the ratio h_o / H. The ratio h_o / H is the quotient between the shallow zone depth, h_o, and the deep zone height, H. The total depth of the channel is h_o + H.

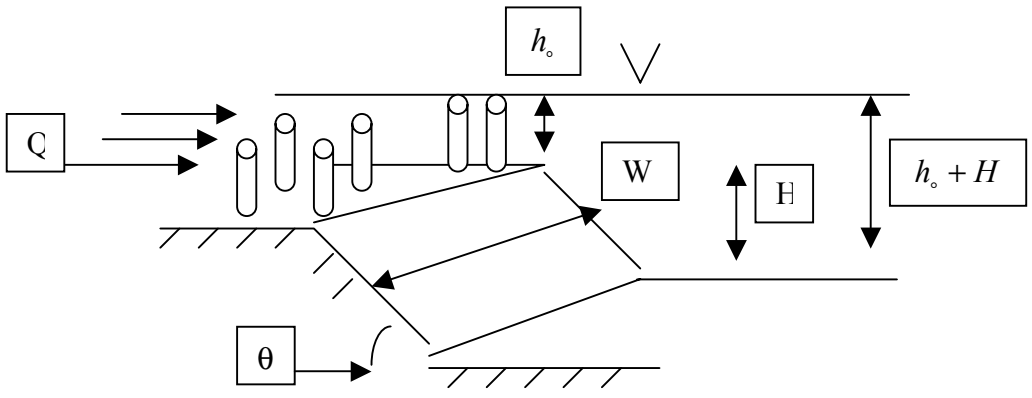

Figure 4(a). - A perspective drawing of the experiment.

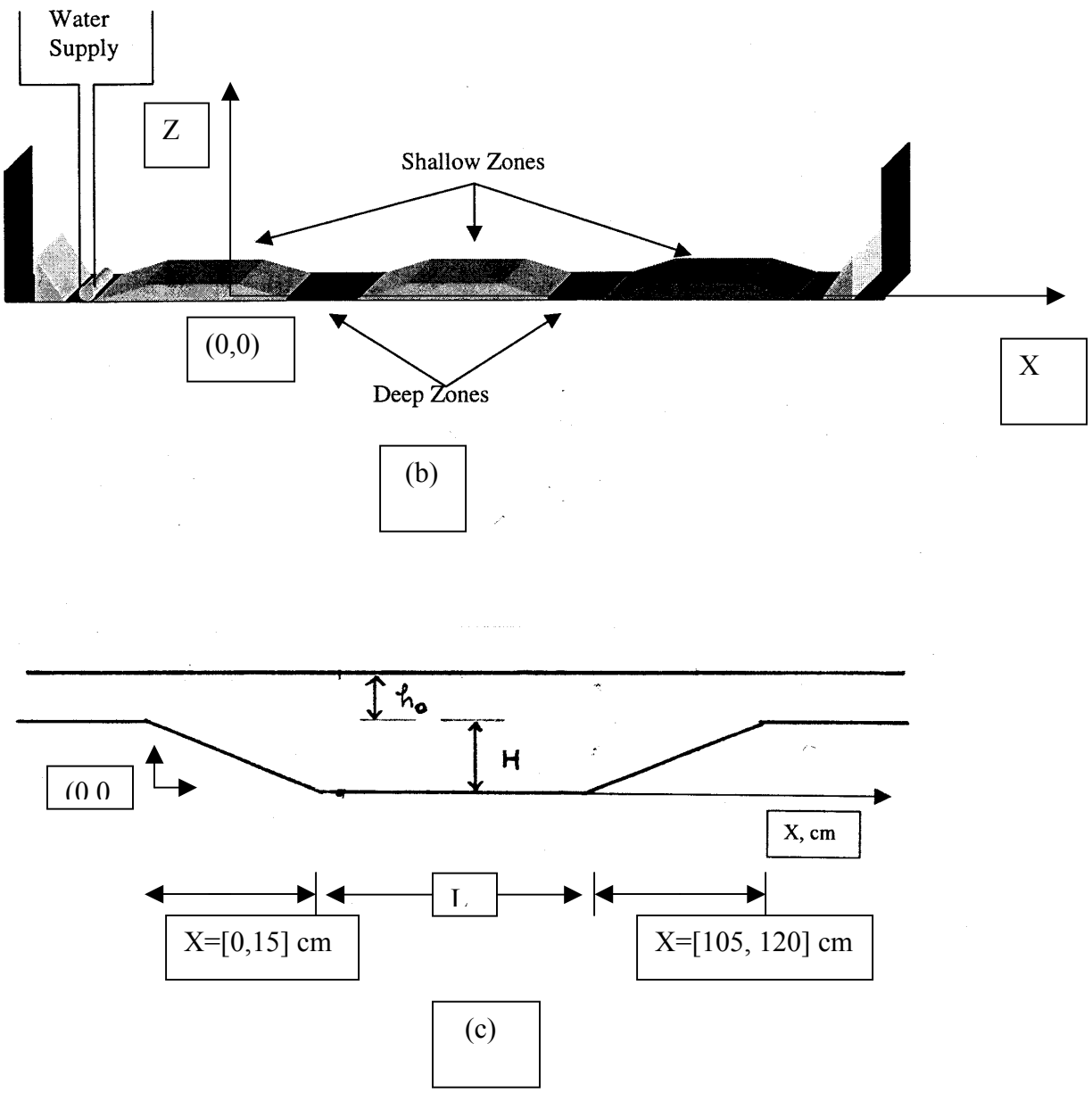

Figure 4. - (b) Experimental schematic arrangement, (c) Experimental coordinate system.

Scaling

The H2 basin located at the Tres Rios Demonstration Wetlands Project site is approximately 244 m long and 61 m wide. It has a series of deep zones and shallow zones, with the deep zones about 3 feet below the shallow zones. The initial set of boxes was designed to simulate the H2 basin, which has three vegetative zones and two deep zones excluding the inlet and outlet deep zones. The horizontal lengths and deep zone

depths were scaled down by a factor of 20 to permit a model with practical dimensions. Since the flow is largely two-dimensional, the effect of the tank's width is assumed to be negligible; the two lateral walls were spaced sufficiently apart to avoid the interaction between boundary layers at the walls.

Reynolds Number Matching

Since the objective of this project was to determine how the deep zone depth and shallow-zone vegetation affect the flow characteristics, it was important that the Reynolds numbers of the model matched the Reynolds number of the actual facility.

The Reynolds number with respect to deep zone depth was defined as:

$$\mathrm{Re}_H = \frac{UH}{\nu}$$

where:

U = shallow-zone velocity $= \frac{Q}{A} = \frac{Q}{h_\circ W(1-S)}$

Q = volumetric flow rate ($\frac{m^3}{\mathrm{sec}}$)

A = cross-sectional area of shallow zone (cm^2)

W = width of channel (cm)

S = solid fraction of vegetation (pegs)

ν = kinematic viscosity of water = $0.0102 \frac{cm^2}{\mathrm{sec}}$

$h_\circ$ = depth of shallow zone

H = depth of deep zone

and can be rewritten for the physical model (W = 40.5 cm, S = 35 percent) as:

$$\mathrm{Re}_H = \frac{Q}{W\nu(1-S)\,h_\circ/H} = C\frac{Q}{h_\circ/H}$$

where:

$$C = \frac{\frac{10^6 cm^3}{1m^3}}{.0102\frac{cm^2}{\mathrm{sec}} \times 40.5cm \times 65\%} = 3.72\times10^6 \frac{\mathrm{sec}}{m^3}$$

The flow rate in the actual facility was estimated to be 18.9 liters per second. Assuming a typical shallow-zone depth of 30.5 cm, a channel width of 61 m, and a porosity of 85 percent, the average shallow-zone velocity U = 0.122 cm/sec. Since the actual step height H from a shallow zone to a deep zone is 91.4 cm, using the above value for the kinematic viscosity of water yields a Reynolds number of 1070 with respect to step height.

The flow rates used in the laboratory experiments ranged from 5.05e-5 to 1.14e-4 m^3/sec. For h_o/H = 0.17, 0.3, and 0.5, these flow rates correspond to Reynolds numbers ranging from 375 to 2210 with respect to the step height.

The Reynolds number with respect to stub diameter is given by:

$$\mathrm{Re}_d = \frac{UD_v}{\nu}$$

where:

U = shallow-zone velocity (same as above)
D_v = stalk diameter (m)
ν = kinematic viscosity of water (same as above)

and can be rewritten for the model (d = 0.009525 m, H = 0.0508) as:

$$\mathrm{Re}_d = \frac{UH}{\nu}\frac{D_v}{H} = \mathrm{Re}_H \frac{D_v}{H} = A\frac{Q}{h_o/H}$$

where: $A = C\frac{D_v}{H} = 6.96\times10^5 \frac{\mathrm{sec}}{m^3}$.

Based on the average stalk diameter of 1.27 cm for a bulrush typical of the H1 and H2 wetlands at the Tres Rios Wetlands Demonstration Project, the Reynolds number is 16. The calculated Reynolds numbers for the model range from 60 to 400. However, both flows are in the same vortex shedding regime and, hence, the laboratory results, when properly scaled, should be applicable to the prototypes at Tres Rios.

Vegetation Modeling

The vegetation in the shallow zones is estimated to have a typical diameter of 1.27 cm and a density of approximately 675 stalks per square meter. This gives a porosity (defined as V_v/V_T where V_V is the volume of the void and V_T is the total volume) of approximately 85 percent.

The construction of the simulated vegetation was as follows: Plastic mats with a scattered grid of holes were fabricated. Then, a random distribution of 65 percent porosity was generated to determine which holes were to be filled. These holes were filled with hot glue and then the mats were attached on top of the shallow zone boxes. Thousands of plexiglas pegs of 0.9525 cm diameter were cut 5.08 cm long and then placed standing vertically in the unfilled holes. The entire process was also repeated for other porosities.

Construction

Original design drawings for the Tres Rios Demonstration Wetlands Project were obtained to accurately simulate the demonstration wetlands with a physical model.

Trapezoidal-shaped boxes were installed in the tank to simulate the vegetated shallow zones while the bottom of the tank simulated the deep zones. Three sets of boxes were constructed, each having a different length, so that the length of the shallow zones and deep zones can be varied during the course of the experiments (figures 5 and 6). The length, L, for each set is as follows: Set I, L = 247.65 cm; Set II, L = 276.86 cm; Set III, L = 287.02 cm. To form the slopes between each shallow and deep zone, three sets of plexiglas wedges were made, each having a different slope. Sets I, II, and III have slopes of 10, 20, and 30 degrees, respectively. With a particular length and slope chosen, the wedges were fastened to the boxes and each unit was fastened to the bottom of the tank.

Water was pumped into the system through a manifold made from 0.5-inch-diameter PVC piping (figure 7). The manifold has six equally spaced discharge points to evenly distribute the influent water similar to the inlet manifolds used in the actual constructed wetlands.

FLOW MEASUREMENTS

Digital-image processing based Particle Tracking Velocimetry (PTV) was used to map the flow fields in the test section. The depth of the shallow zone to that of the deep zone was maintained at the minimum level $h_o / H = 0.1316$. The deep zone was divided into eight sections (windows) of size 15 x 7.0 cm for imaging, and velocity records taken in the windows were later amalgamated to synthesize the entire flow field.

Before the measurements, the flow was allowed to reach a steady state. Pliolite particles of size 100-150 microns were added to the flow, and their motions were tracked in each window by a super VHS camera. The images so taken were post-processed using the DIGIMAGE software, and the particle tracks in the video frames were used to calculate the velocity field using digital imaging techniques.

The two-dimensional velocity field for a flow rate of 3.4 gpm and a ratio of $h_o/H = 0.1316$ is shown in figure 8(a). In this figure, we show four windows that represent the subzones where maximum and minimum velocities occur due to the very nature of the flow geometry. Window I shows the slope from x = 0 to x = 15.0 cm, where x is measured along the water surface with x = 0 at the end of the shallow zone. Note the upper level flow where the velocity is almost uniform and the lower re-circulation zone with low velocities. Window II is in the flat part of the deep zone from x = 45.0 to x = 60.0 cm, while window III is from x = 60.0 to x = 75.0. The second and third windows show minimum velocity in the flow system. The last window is from x = 105.0 to x = 120.0 cm, wherein the flow approaches the far end slope of the deep zone. Note that this region represents an upslope flow, with very little recirculation. The mass conservation

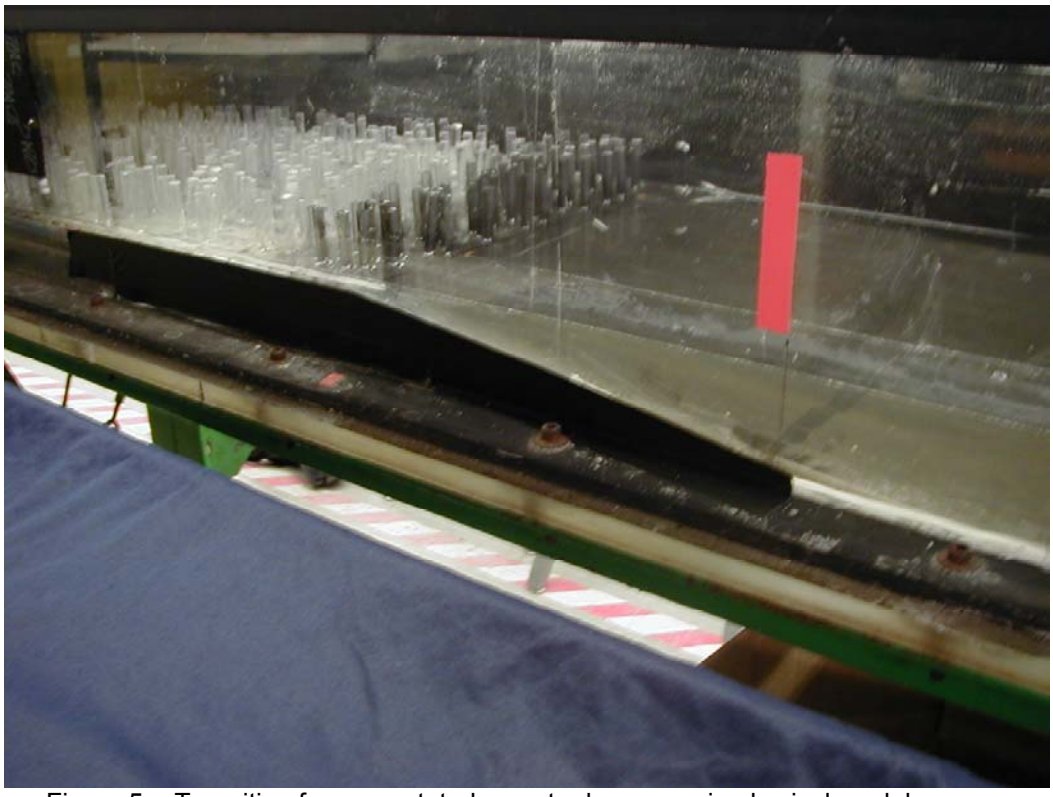

Figure 5. - Transition from vegetated zone to deep zone in physical model.

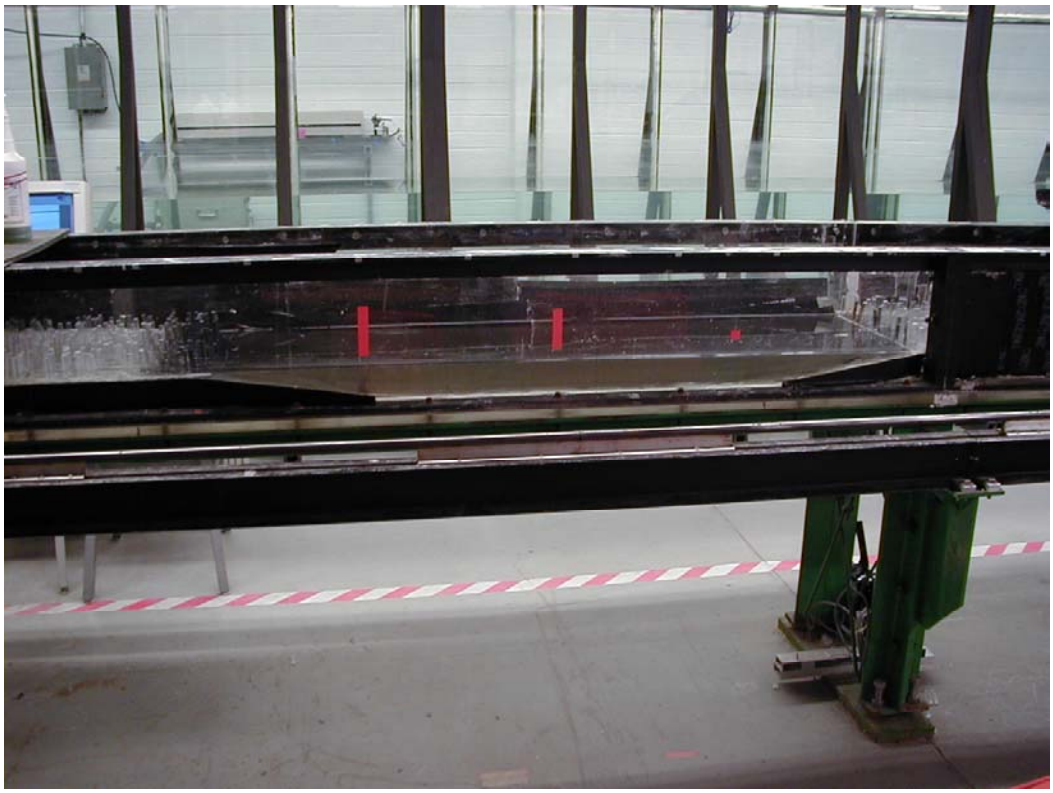

Figure 6. - Deep zone section of physical model. The red tape delineates the length of an observation.

Figure 7. - Physical model with influent water tank and flow controller at forefront.

in this region requires the flow to accelerate before entering the shallow zone. Figures 8(b) and 8(c) are similar to figure 8(a), in which flow rates 2.5 gpm and 1.8 gpm are shown. Comparisons between these pictures indicate that flow patterns remain the same in spite of the variations in flow rate. The experimental runs completed with different flow rates (q) and the pertinent parameters are shown in tables 5-8. These tables present the matrix of experiments that were performed.

In figures 8(a) 8(b), and 8(c), the length of the arrow above each window represents a velocity vector whose magnitude is 5 cm/s. This is the velocity scale for the velocity maps. Arrow lengths give the magnitude of the velocity vectors in each window. These are a multiple of the 5 cm/s velocity vector length. This means that the average velocity at a given position X is between 0 and 5 cm/s. Velocity vectors in windows I and IV slant, due to the presence of slopes and eddies in these regions. Velocity vectors are bigger and bolder where the acceleration or slowing down is stronger due to the geometry and to conserve mass and energy.

The next stage of experiments was focused on PTV and on the determination of transport coefficients in the shallow zone. These were low velocity experiments with speeds less than 1 cm/s at the surface. A random distribution of pegs installed in the shallow zone and the dispersion of a passive scalar introduced into the system was studied using laser-induced fluorescence and particle tracking velocimetry techniques.

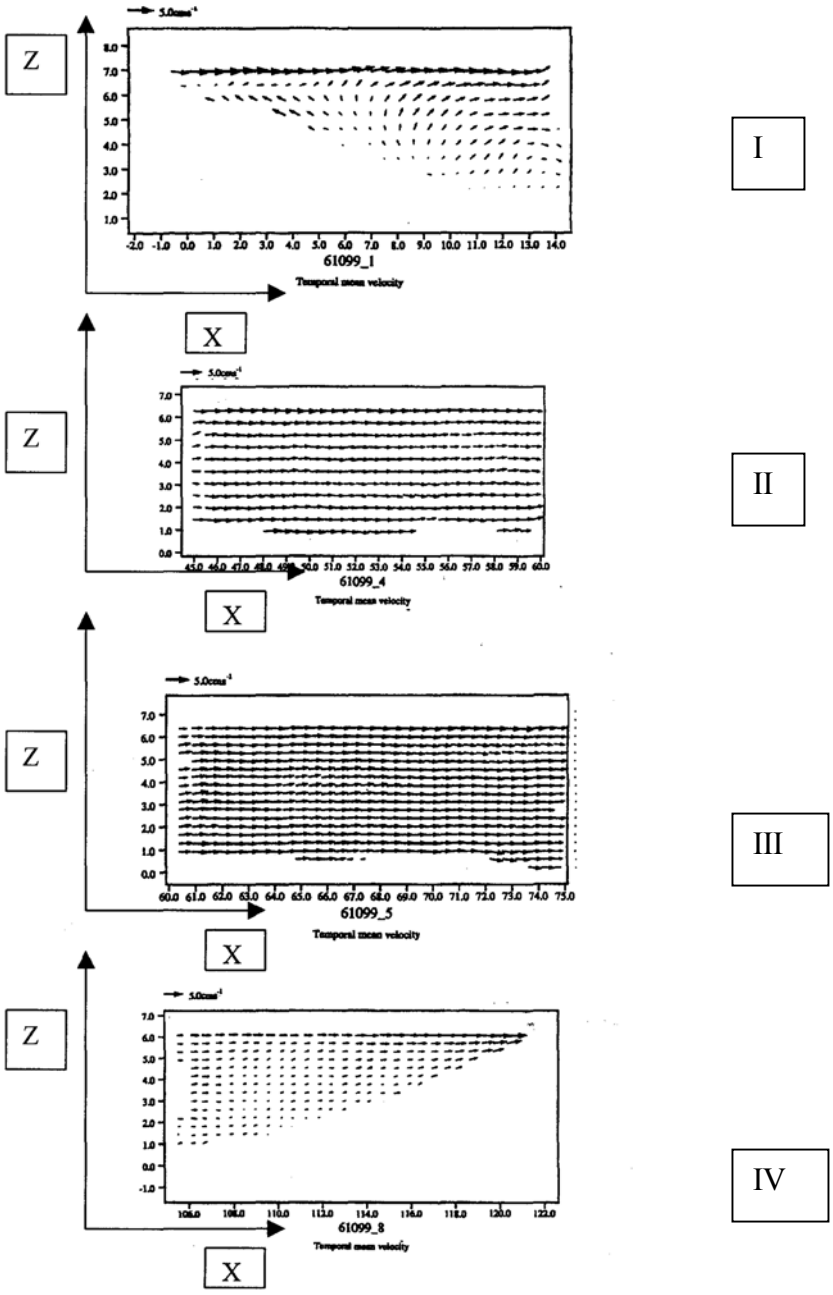

Figure 8(a). - Vector velocity field for a flow rate of 3.4 gpm and $h_o/H = 0.1316$ (minimum level).

Two types of velocity measurements were carried out, namely, the surface velocity measurements and whole-field measurements. The surface velocity was measured to obtain an idea of the aerial velocity field of the wetland, and the measurements consisted of tracking suspended particles on the surface by a downward-looking video camera. The channel was isolated from the background laboratory perturbations by isolating the experimental apparatus by a set of screens. In this method, the surface velocity, Vs, for a given experiment was calculated from the stream-wise distance X versus t data. Whole-field velocity measurements were done by applying particle tracking velocimetry.

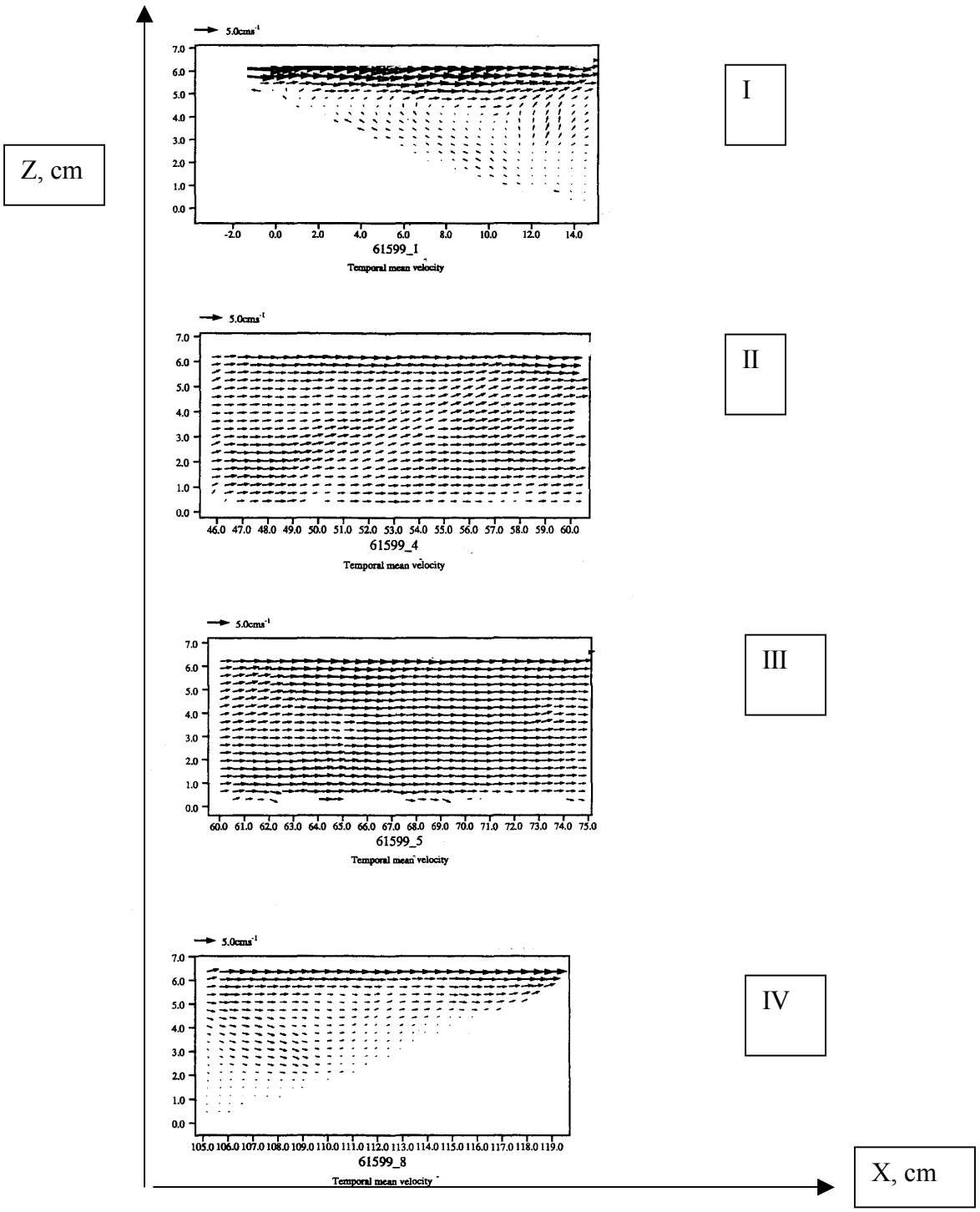

Figure 8(b). - Vector velocity field for a flow rate of 2.5 gpm and $h_o/H = 0.1316$ (minimum level).

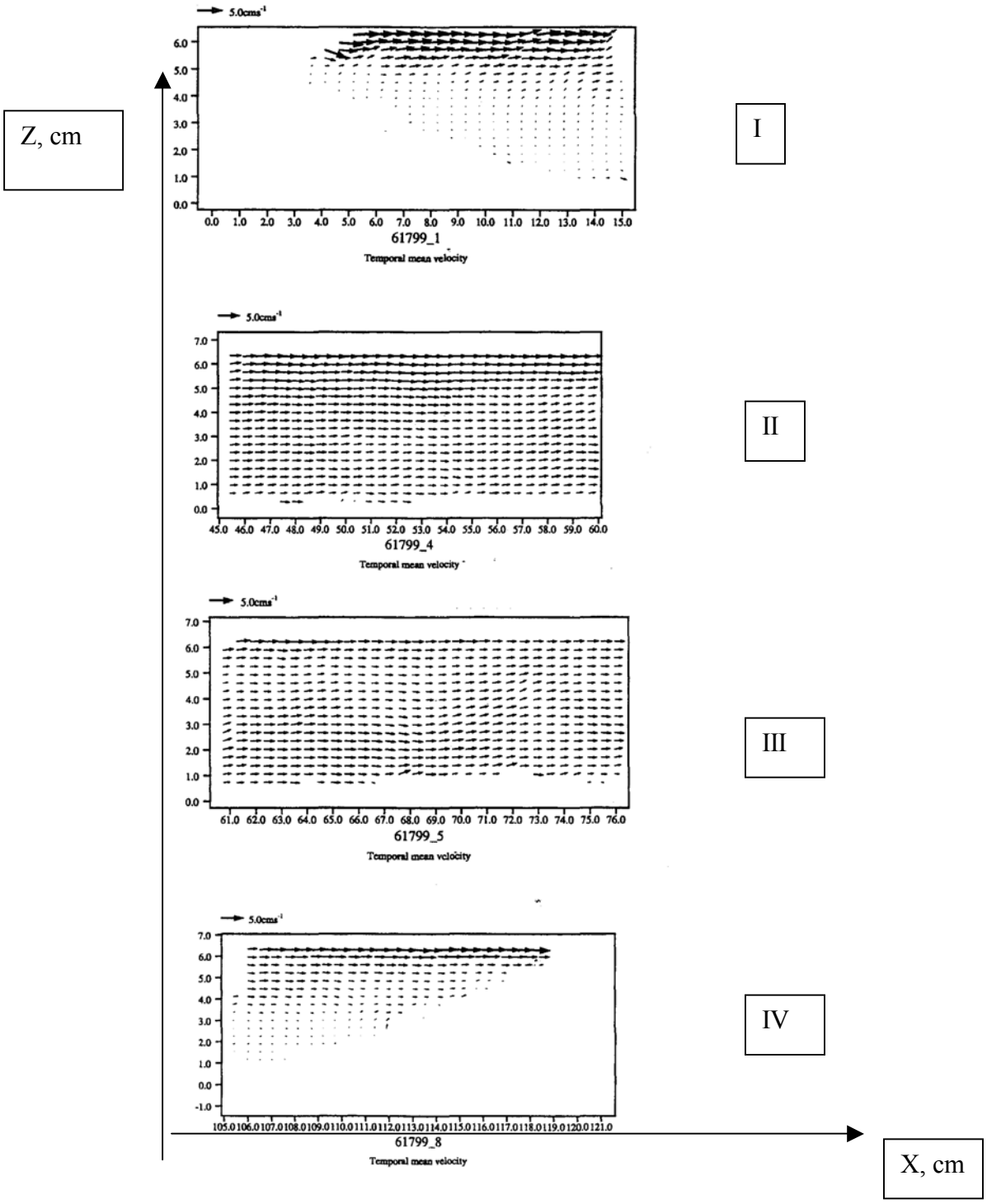

Figure 8(c). - Vector velocity field for a flow rate of 1.8 gpm and $h_o/H = 0.1316$ (minimum level).

Table 5. - Number of runs completed. (In this table, the section columns identify each run with the date and the experiment number.)

Runs Completed

Side View $\theta = 20^\circ$ S = 35 %

h/H	q (gal/min)	Section 1	Section 2	Section 3	Section 4	Section 5	Section 6	Section 7	Section 8
0.17	1.6	**120499_1**	120499_2	120499_3	120499_4	120499_5	120499_6	120499_7	120499_8
0.17	1.3	**120599_1**	120599_2	120599_3	120599_4	120599_5	120599_6	120599_7	120599_8
0.17	1.15	**120899_1**	120899_2	120899_3	120899_4	120899_5	120899_6	120899_7	120899_8
0.17	1	**120699_1**	120699_2	120699_3	120699_4	120699_5	120699_6	120699_7	120699_8
0.17	0.8	**120799_1**	120799_2	120799_3	120799_4	120799_5	120799_6	120799_7	120799_8
0.3	1.8	**013100_1**							
0.3	1.6	**120999_1**	**120999_2**	**120999_3**	**111799_4**	**111799_5**	**111799_6**	**111799_7**	**111799_8**
0.3	1.3	**111899_7**	**111899_6**	**111899_5**	**111899_4**	**111899_3**	**111899_2**	**111899_1**	**111799_9**
0.3	1.15	**112099_6**	**112099_7**	**112099_8**	**112099_9**	**112199_1**	**112199_2**	**112199_3**	**112199_4**
0.3	1	**111899_8**	**111899_9**	**111999_1**	**111999_2**	**111999_3**	**111999_4**	**111999_5**	**111999_6**
0.3	0.8	**112099_5**	**112099_4**	**112099_3**	**112099_2**	**112099_1**	**111999_9**	**111999_8**	**111999_7**
0.5	1.8	**020100_1**							
0.5	1.6	**112999_8**	**112999_7**	**112999_6**	**112999_5**	**112999_4**	**112999_3**	**112999_2**	**112999_1**
0.5	1.3	**113099_1**	113099_2	113099_3	113099_4	113099_5	113099_6	113099_7	113099_8
0.5	1.15	**120199_1**	120199_2	120199_3	120199_4	120199_5	120199_6	120199_7	120199_8
0.5	1	**120299_1**	120299_2	120299_3	120299_4	120299_5	120299_6	120299_7	120299_8
0.5	0.8	**121099_1**	121099_2	121099_3	121099_4	121099_5	121099_6	121099_7	121099_8

*Bold face signifies tracking done and film produced.

Table 6. - Number of runs completed. (The run number is identified by the date and the experiment number.)

Runs Completed

Side View Section 1

h/H	q (gal/min)	$\theta = 20^\circ$ S=10%	$\theta = 10^\circ$ S=10%	$\theta = 10^\circ$ S=35%	$\theta = 30^\circ$ S=35%	$\theta = 30^\circ$ S=10%
0.17	1.6	033000_1				
0.17	1.3	033000_2				
0.17	1	033000_3				
0.17	0.8	033000_4				
0.3	1.8	033100_1				
0.3	1.6	033100_2				
0.3	1.3	033100_3				
0.3	1	033100_4				
0.3	0.8	033100_5				
0.5	1.8	**040100_1**				
0.5	1.6	**040100_2**				
0.5	1.3	**040100_3**				
0.5	1	**040100_4**				
0.5	0.8	**040100_5**				

*Bold face signifies tracking done and film produced.

Table 7. - Number of runs completed. (In this table the section columns identify each run with the date and the experiment number.)

Runs Completed

Top View $\theta = 20^\circ$ S = 10 %

h/H	*q (gal/min)*	*Section 1*	*Section 3*	*Section 5*	*Section 6*	*Section 8*
0.5	*1.8*	**032100_1**	**032100_3**	032100_5	032100_6	032100_8
0.5	*1.6*	031700_1	031700_3	031700_5	031700_6	031700_8
0.5	*1.3*	031800_1	031800_3	031800_5	031800_6	031800_8
0.5	*1*	031900_1	031900_3	031900_5	031900_6	031900_8
0.5	*0.8*	032000_1	032000_3	032000_5	032000_6	032000_8
0.3	*1.8*	032200_1	032200_3	032200_5	032200_6	032200_8
0.3	*1.6*	032300_1	032300_1	032300_1	032300_1	032300_1
0.3	*1.3*	032300_1	032300_1	032300_1	032300_1	032300_1
0.3	*1*	032400_1	032400_3	032400_5	032400_6	032400_8
0.3	*0.8*					
		032500_1	032500_3	032500_5	032500_6	032500_8
0.17	*1.6*	032600_1	032600_3	032600_5	032600_6	032600_8
0.17	*1.3*	032700_1	032700_3	032700_5	032700_6	032700_8
0.17	*1*	032800_1	032800_3	032800_5	032800_6	032800_8
0.17	*0.8*	032900_1	032900_3	032900_5	032900_6	032900_8

*Bold face signifies tracking done and film produced.

Table 8. - Number of runs completed. (In this table the section columns identify each run with the date and the experiment number.)

Runs Completed

Top View $\theta = 20^\circ$ S = 35 %

h/H	*q (gal/min)*	*Section 1*	*Section 3*	*Section 5*	*Section 6*	*Section 8*
0.17	*1.6*	**022700_1**	**022700_3**	**022700_5**	**022700_6**	**022700_8**
0.17	*1.3*	**022800_1**	**022800_3**	**022800_5**	**022800_6**	**022800_8**
0.17	*1*	**022900_1**	**022900_3**	**022900_5**	**022900_6**	**022900_8**
0.17	*0.8*	**030100_1**	**030100_3**	**030100_5**	**030100_6**	**030100_8**
0.3	*1.6*	**030200_1**	**030200_3**	**030200_5**	**030200_6**	**030200_8**
0.3	*1.3*	**030300_1**	**030300_3**	**030300_5**	**030300_6**	**030300_8**
0.3	*1*	**030400_1**	**030400_3**	**030400_5**	**030400_6**	**030400_8**
0.3	*0.8*	**030500_1**	**030500_3**	**030500_5**	**030500_6**	**030500_8**
0.5	*1.8*	**030600_1**	**030600_3**	**030600_5**	**030600_6**	**030600_8**
0.5	*1.6*	**030700_1**	**030700_3**	**030700_5**	**030700_6**	**030700_8**
0.5	*1.3*	**030800_1**	**030800_3**	**030800_5**	**030800_6**	**030800_8**
0.5	*1*	**030900_1**	**030900_3**	**030900_5**	**030900_6**	**030900_8**
0.5	*0.8*	**031000_1**	**031000_3**	**031000_5**	**031000_6**	**031000_8**

*Bold face signifies tracking done and film produced.

Necessary hardware for the PTV included a super-VHS video recorder, video monitor, Pentium IBM-PC compatible with frame grabber card and Dig Image, an integrated image processing software package developed at Cambridge University, U.K. A CCD video camera recorded the movement of neutrally buoyant polystyrene particles, which were illuminated as they passed through a two-dimensional vertical light sheet (approximately 1 cm or 5 cm thick). After the experiment, by digitizing consecutive frames of images, the particle velocities were calculated by dividing the distance a particle moved from frame to frame by the time increment between frames. Large particle concentrations were used to obtain instantaneous velocity and velocity derivatives of the entire field of view.

Recording rate was 30 frames per second (60 fields) onto a Maxwell SVHS tape. The CCD was focused on the desired region (e.g., along one slope of the deep zone), and a variable light shutter was adjusted to ensure that the intensity of digitized images was not saturated.

In order to record particle trajectories over a period of time, reference points and a laboratory coordinate system were added to the experiment. Four 1.5V LED's connected in series were used as reference points to locate common points from frame to frame on the videotape. An adjustable voltage source was used to decrease the LED brightness so as not to saturate their intensity level on the digitized image.

Before each experiment, a grid, etched on a thin sheet of plexiglas, was inserted into the flow field and illuminated by the light sheet to record the laboratory coordinate system of the experiment. Measured grid locations were input into the tracking software to transform laboratory coordinates to the pixel coordinates of a digitized image.

During the experiments, due to experimental constraints, the deep zone was divided into several windows. The typical size of each window was 15.0 x 7.0 cm. Schematics of the flow configuration used and imaging windows are shown in figure 2b, and the specifications of windows used are given in tables 7 and 8. The experiment was allowed to run for about 30 minutes to allow the flow to achieve steady-state conditions before velocity measurements were initiated.

Table 9 presents PTV experiments conducted with a fixed level, $h_o/H = 0.1316$ (minimum level), three flow rates and four observation windows. Numbers presented in the table are data files.

Table 9. – PTV experiments conducted with a fixed level, $h_o/H = 0.1316$

Flow Rate/ Window	W1=[0,15]cm	W2=[45,60]cm	W3=[60,75]cm	W4=[105,120]cm
1.8 gpm	61799_1	61799_4	61799_5	61799_8
2.5 gpm	61599_1	61599_4	61599_5	61599_8
3.4 gpm	61099_1	61099_4	61099_5	61099_8

Table 10 presents PTV experiments conducted at a fixed flow rate of 1 gpm, three levels and three observation windows. For these series of experiments, we only processed 3 windows because there was not significant change in the velocity magnitude and direction between windows 3 and 4 in previous experiments. Numbers presented in the table are data files.

Table 10. - PTV experiments conducted at fixed flow of 1 gpm

Level\Window	W1=[0,15] cm	W2=[45,60] cm	W3=[105,120] cm
$h_o/H = 0.2$	110599_7	110599_8	110599_9
$h_o/H = 0.26$	1109994C	1109995b	1109996b
$h_o/H = 0.4$	110599_1	110599_2	1109993C

SIMPLIFIED MODEL FOR WETLAND HYDRODYNAMICS

To facilitate the interpretation of experimental results on flow and dispersion, a simple model was developed to explain various hydrodynamic features of wetlands. Each zone was treated separately, as discussed below.

SHALLOW ZONE

For simplicity, consider a wetland consisting of uniformly distributed plants, separated by a distance d_v, as shown in figure 9. Essential parameters used in the theoretical model are represented. The number of plants surrounding a given plant (emergent vegetation) depends on the geometry of the array, but for all cases the number of shoots per unit area S can be related to d_v as

$$S_A \propto 1/ d_v^2 \qquad \textbf{(1)}$$

For example, for a hexagonal array, $S_A = 2 /(3^{1/2} d_v^2)$, and for a square array, it can be shown that $S_A = 1/ d_v^2$. Therefore, in general, it is possible to specify the vegetation in a wetland by the three parameters d_v, D_v (the diameter of emergent vegetation), and a geometric factor G that takes into account the pattern of vegetation distribution. For a random distribution of vegetative elements (figure 10), G is fixed and numerical computations confirm $S_A \propto 1/ d_v^2$.

In parameterizing the flow throughout the vegetation, it is instructive to consider the hydrodynamics of a single element and then infer the combined influence of the entire shrub population. As evident from figure 10, each shoot modifies the flow surrounding it, and the nature of modification depends on the Reynolds number $Re_d = UD_v/\nu$, where

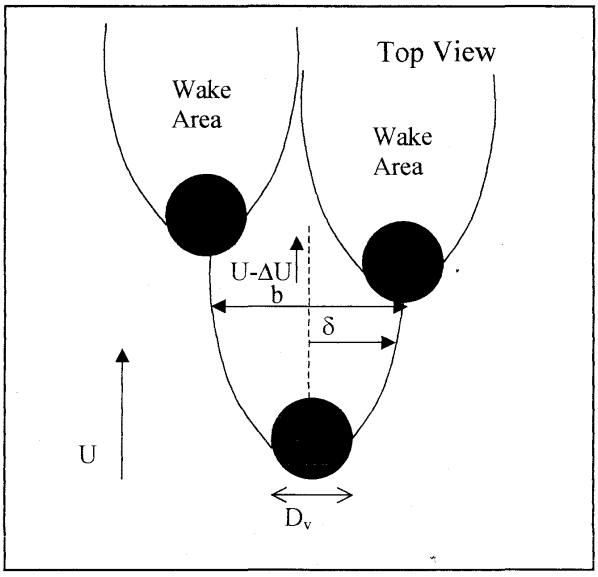

Figure 9. – Schematic top view of the wakes generated by the cylinders.

ν is the kinematic viscosity. The nature of flow past a single cylindrical element in the absence of other elements is well known, wherein it has been shown that flow at $Re_d < 1$ (creeping flow) consists of simple displacement of streamlines (without any eddies or vortices), and for $5 < Re_d < 60$, the laminar flow separates downstream of the cylinder with a pair of attached vortices to the shrub. At $60 < Re_d < 5000$, the vortex wake tends to oscillate and then break down into well-organized patterns (Karman vortex streets). For $Re_d > 5000$, there is no simple laminar vortex shedding, and the turbulent flow appears in the wake. Whether the same phenomenon occurs in a region of emergent vegetation with submerged tree vegetation is not clear, but one may expect different wake flow dynamics in different Re_d ranges.

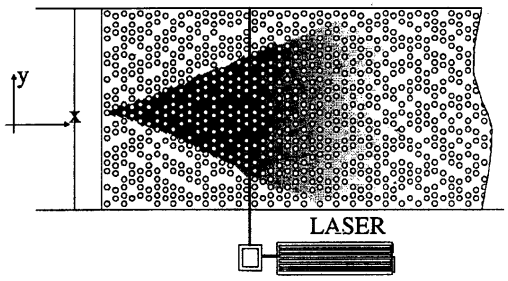

Figure 10. - A random array of vegetative elements and the dispersion of dye.

A phenomenon that is common to all of the above regimes is the drag force exerted by vegetation. Therefore, we will model the influence of vegetation on the flow as drag forces F_D due to a large number of drag elements placed in the flow. By approximating the flow to be homogenous in the bulk of the submerged region the available drag laws

can be used to estimate the influence of vegetation. As shown in figure 9, the drag induced by vegetation can be related to the characteristic velocity deficit in the wake ΔU at a downstream location where the wake width is b, viz.,

$$F_D = (U\Delta U)b \ , \tag{2}$$

and, hence, the defect velocity ΔU can be written in terms of the drag coefficient.

$$C_D = F_D / \frac{1}{2}\rho U^2 D \quad \text{as} \quad C_D = \left(\frac{\Delta U}{U}\right)\left(\frac{b}{D_v}\right). \tag{3}$$

Note that (3) specifies the influence of a single vegetative element on the flow. Since the wake of a given element interacts with a downstream element located at a distance of order d_v, the realm of hydrodynamic influence of each element can be thought as extending to a length scale d_v. Therefore, the lateral velocity scale induced by a shrub can be estimated as

$$V \sim \frac{\Delta U b}{d_v} \sim C_D U \frac{D_v}{d_v} \sim C_D U D_v \sqrt{S_A} \tag{4}$$

The lateral dispersion depends on V as well as the lateral length scale of the flow. Two possible candidates for this lateral scale are the vegetative diameter D_v and the thickness of the wake. Near an element, the wake width is D_v, but it grows in the laminar flow region according to the well known formula $d\delta \propto (\nu x / U)^{1/2}$, where $d\delta$ is the incremental growth of the wake thickness beyond D_v and x is the downstream distance. In cases where the vegetation is densely distributed, then the wake growth between two elements $(\nu d_v / U)^{1/2}$ is small compared to the element diameter, D_v or $d_v / D_v < Re_D^2$, D_v can be considered as the most appropriate candidate. Then, the transverse eddy diffusivity $K_T \propto VD_v$ can be written as

$$K_T = \beta C_D U \frac{D_v^{\ 2}}{d_v} = \beta C_D U D_v \sqrt{S_A} \tag{5}$$

where β is a universal constant. The Reynolds number dependence in (5) enters through C_D, which also can be written in the form of

$$K_T / UD_v = \beta [C_D (Re_D)](D_v / d_v) \tag{6}$$

The drag on infinitely long cylinders has been investigated extensively. An analytical solution exists for $Re_D < 1$, in the form (Lamb 1932, Hydrodynamics, Dover)

$$C_D = 8\pi\, Re_D^{-1} \frac{1}{\left(\frac{1}{2} - \gamma - log\frac{Re}{4}\right)}, \tag{7}$$

but there are no solutions for higher Re_D. The drag data for the attached vortex and vortex shedding regimes can be fitted to the following formulae

$$C_D = 4.53\, Re_D^3 - 1.3\, Re_D^2 + 0.022\, Re_D - 1.36x10^{-5} \quad \text{for } 5<Re_D<60 \tag{8}$$

and

$$C_D = 1.2 \qquad \text{for } 60<Re_D<5000$$

which can be used in evaluating K_T using (5).

DEEP ZONE DYNAMICS

Deep zones are employed to reduce the effects of flow inhomogeneities formed during the passage of flow through the shallow zone. Such inhomogeneities mainly arise due to the development of low resistance channels in the shallow zone, which can be attributed to the defunction of plants. The bordering region between the vegetation and open waters is subjected to increased shear stress, causing the plants in the frontier to be subject to extra strain and perhaps to ultimate removal. The development of low resistance paths in regions devoid of plants, therefore, is a self-promoting mechanism and, hence, unavoidable in constructed wetlands. Such paths reduce the contact time between the flow and the plants and soil, causing severe operational problems in wetlands.

The flow in low resistance paths emerges out of the vegetation zone as narrow streams, say, with a characteristic width ℓ. If the depth of the flow were to be uniform, then these narrow streams are expected to be dissipated with a time scale ℓ^2 / ν. The presence of the deep zone, however, causes these streams to dissipate much faster, as it allows the vorticity associated with the streams to demise via a combined stretching and viscous diffusion mechanism. The dissipation of vorticity in the deep zone is a key factor in establishing a uniform flow for the next shallow zone. As a first step in estimating the time and length scales of dissipation, the inhomogeneities due to streams were modeled as vortices of shear layers bounding the streams. The vortices entering the deep zone amplify by stretching, governed by the balance $d\omega_z / dt \sim \omega_z\, \partial w/\partial z$, where ω_z is the vorticity, z is the vertical coordinate and w is the vertical velocity. Since $\partial w/\partial z = \alpha U(x)/$

h(x), where h (x) and U (x) are the local water depth and average flow velocity, respectively, and α is the slope of the walls, it is possible to write

$$\frac{1}{\omega_Z}\frac{d\omega_Z}{dt} = \frac{\alpha U_0 h_0}{(h+\alpha x)^2}. \tag{9}$$

The advection of vortex by the flow can be represented by

$$\frac{dx}{dt} = \frac{U_0 h_0}{(h_0+\alpha x)}, \tag{10}$$

where x is the distance traveled in the deep zone. It should be noted that the flow in the deep zone can be complex, and the representation of flow in it by a single uniform velocity can be criticized as an oversimplification of the problem. However, as a first step in estimating the deep zone processes, this assumption is reasonable. Equations (9) and (10), together with the mass and angular momentum conservation in vortices,

$$r_0^{\,2} w_0 = r^2 w$$

and

$$r_0^{\,2} h_0 = r^2 (h_0+\alpha x) = r^2 h(x), \tag{11}$$

where r and h are the radius and height of the vortices and subscript o denotes the initial conditions at x = 0, can be used to estimate the local vorticity $\omega(z)$ at a time t after entering the deep zone and the rate of contraction of vortex $U_c = dr / dt$ as

$$\omega_z = \omega_0\left(1+\frac{\alpha U_0 t}{h_0}\right),$$

and

$$U_c = -\frac{\alpha r_0 U_0}{2h_0}\frac{(1+\alpha x/h_0)^{\frac{1}{2}}}{(1+\alpha x/h_0)^3}. \tag{12}$$

$$\omega_z = \omega_0\left(1+\frac{\alpha U_0 t}{h_0}\right),$$

The vortices are expected to dissipate rapidly by the viscosity when the rate of contraction of the vortex U_c becomes of the same order as the rate of viscous diffusion, ν/r or at a distance

$$x \approx \left(\frac{h_o}{\alpha}\right)^3 \sqrt{\frac{\alpha r_o^{\,2} U_o}{2h_o \nu}} = \beta_1 \left(\frac{h_o}{\alpha}\right) \sqrt{\frac{\alpha r_o^{\,2} U_o}{2h_o \nu}} = \gamma \tag{13}$$

where the limit $x > h_0 / \alpha$ has been assumed.

Therefore, in design of wetlands, the depth of the deep zone for a given α ought to be selected according to

$$H = \gamma \left(\alpha^2 h_o\right)^3 \sqrt{\frac{\alpha r_o^{\,2} U_o}{2h_o \nu}} \tag{14}$$

RESULTS AND DISCUSSION

NATURE OF THE FLOW

As stated earlier, two major governing variables describing the nature of wetland flow are the Reynolds number based on the deep zone depth $Re_H = UH/\nu$ and that Re based on the vegetative diameter Re_d, and the ratio h_o/H. In dealing with the deep zone, the influence of Re_d can be considered secondary and, hence, the important variables are Re_H and h_o/H. In the experiments, it was found that the flow in the deep zone is quite sensitive to these variables.

For large Re_H and smaller h/H, the flow leaving from the shallow zone to the deep zone exhibited separation at the slope and a secondary flow built up in response to the separation. This is shown in figure 11 where the vorticity for different flow rates and h_o/H are shown, plotted as distance (x-axis) against height (y-axis), for S = 35 percent (S = solid fraction of vegetation) and slope angle 20^o. The color red represent the highest vorticity. The slope angle α is also denoted as θ. Note the appearance of vorticity at the slope with increasing flow rate (Re_H) for a given h_o/H and the strengthening of the vorticity with increasing h_o/H for a given flow rate. A similar trend was observed for S = 10 percent and $\theta = 20^o$, as shown in the figure 12. The results for $\theta = 20^o$ and S = 35 percent are shown in figure 13 as a regime diagram between Re_H and h_o/H. Note the presence of a threshold curve in the Re_H - h_o/H plane that separates the recirculation and non-recirculation regimes which can be used for future designs. Figure 14 shows the top view of the flow, indicating how the vorticity generated at the shallow (vegetated) zone disappears in the deep zone. For high flow rates, the vorticity persists for some time, whereas the vorticity generated by vegetation is decayed somewhat quicker at slow

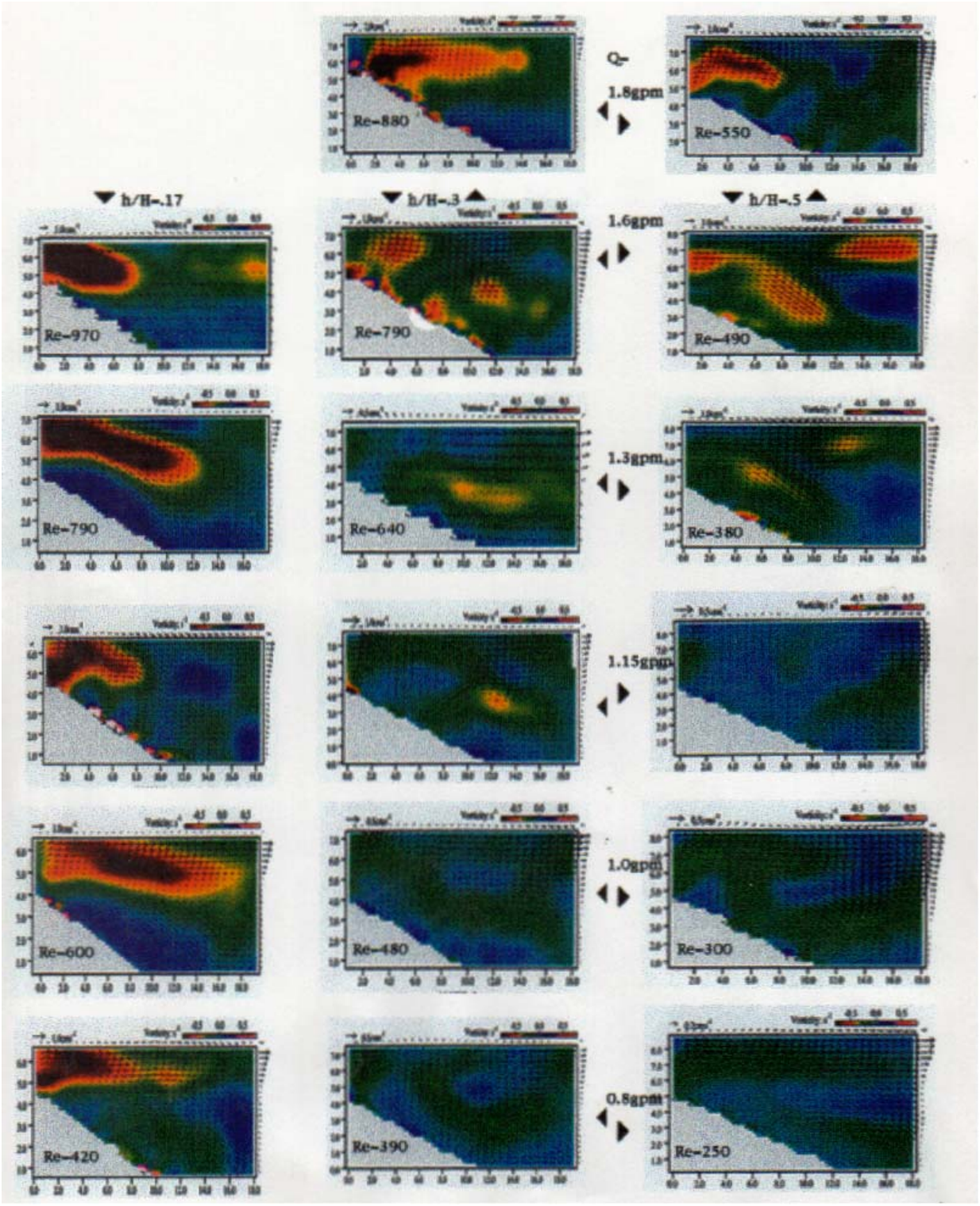

Figure 11. - Velocity maps. Side view with S = 35 percent and θ = 20 degrees.

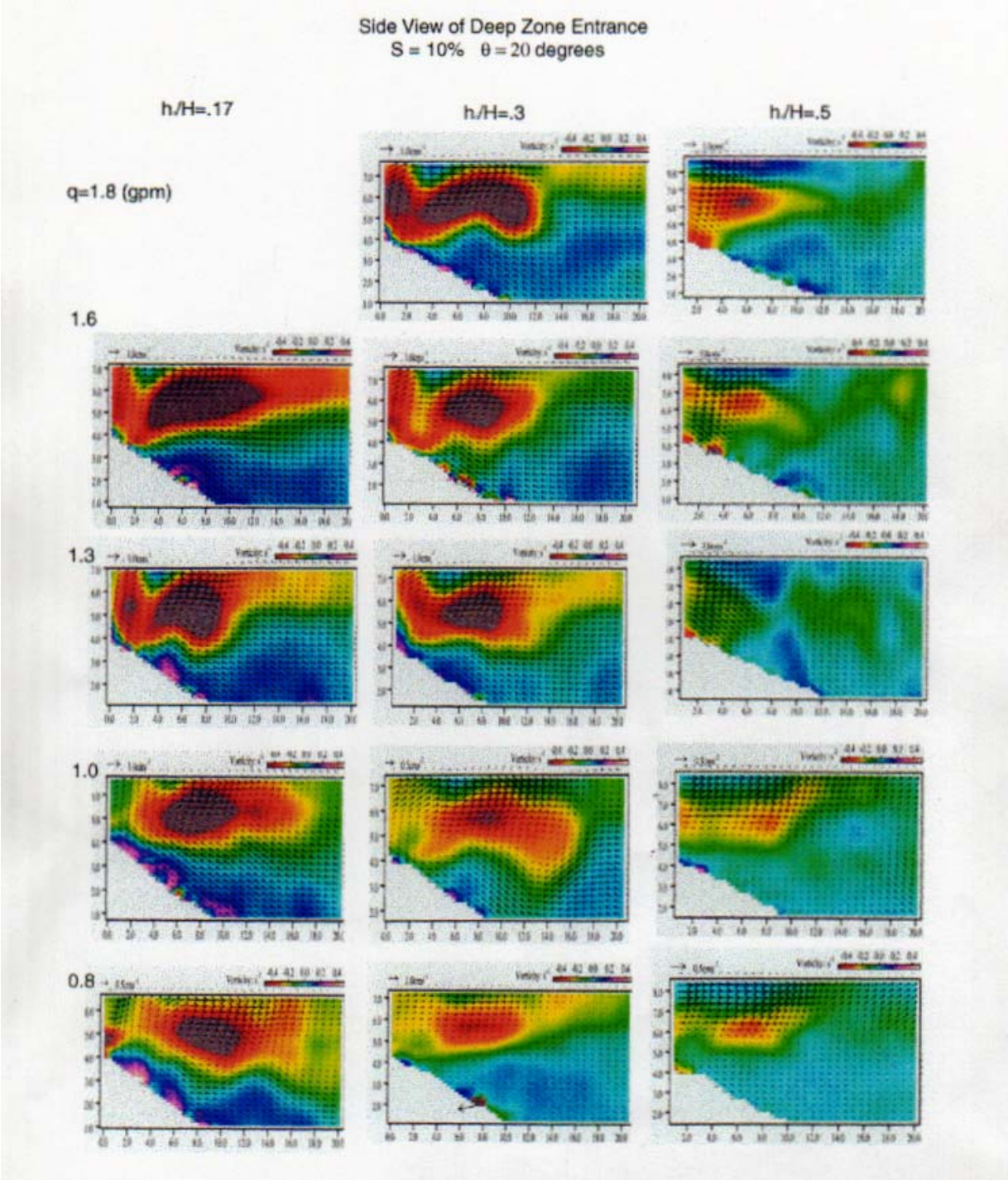

Figure 12. - Velocity maps corresponding a side view of deep zone entrance.
S = 10 percent and θ = 20 degrees.

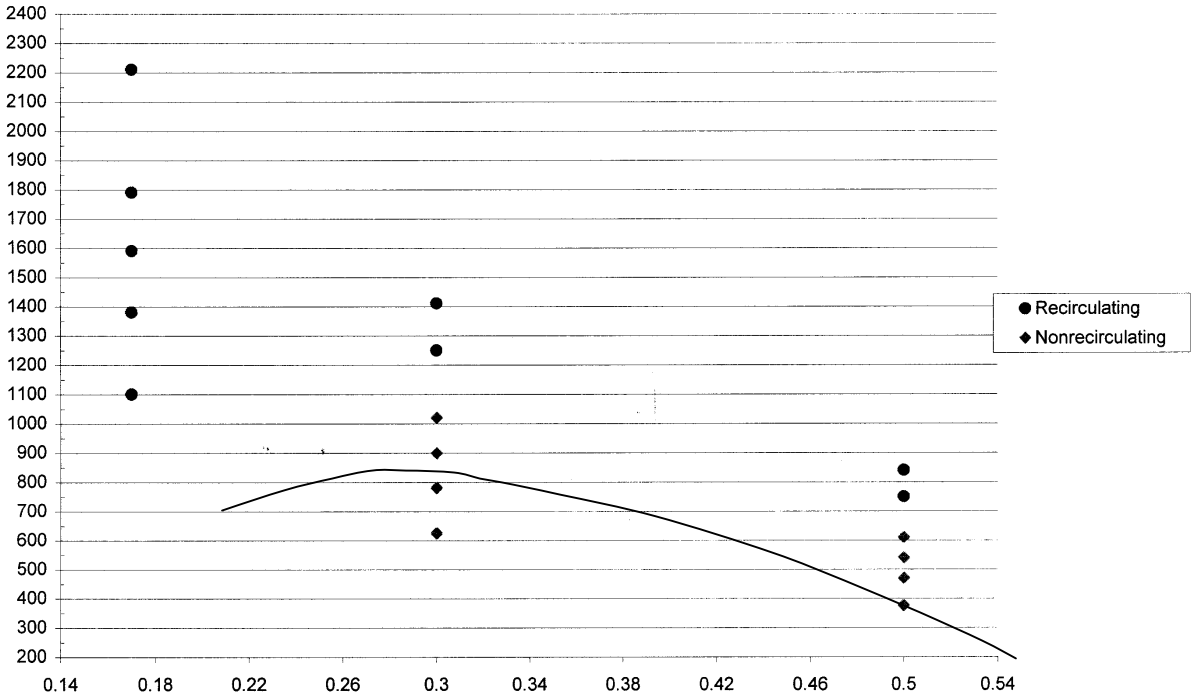

Figure 13. - Effects of ReH versus h/H on deep zone recirculation.
S = 35 percent and θ = 20 degrees.

flow rates. This agrees with equation 14, which shows that the length where the effects of vegetation should disappear increases with the square root of the velocity in the vegetation zone.

MEASUREMENTS OF LATERAL DISPERSION COEFFICIENT

The lateral dispersion coefficient within the vegetation zone was measured by injecting fluorescent dye at some distance into the cylinder array (measured from the inlet to the shallow zone); see figures 15 and 10. The spreading of this fluorescent plume was then monitored from above (imaging the x-y plane) for about 2 minutes under the illumination of a horizontal laser beam. The experiments were then repeated by changing the position of the dye injection point along the long axis of the vegetated zone. The instantaneous distributions of dye at different downstream distances from the source were then analyzed and the instantaneous frames were then ensemble averaged to obtain the mean profile.

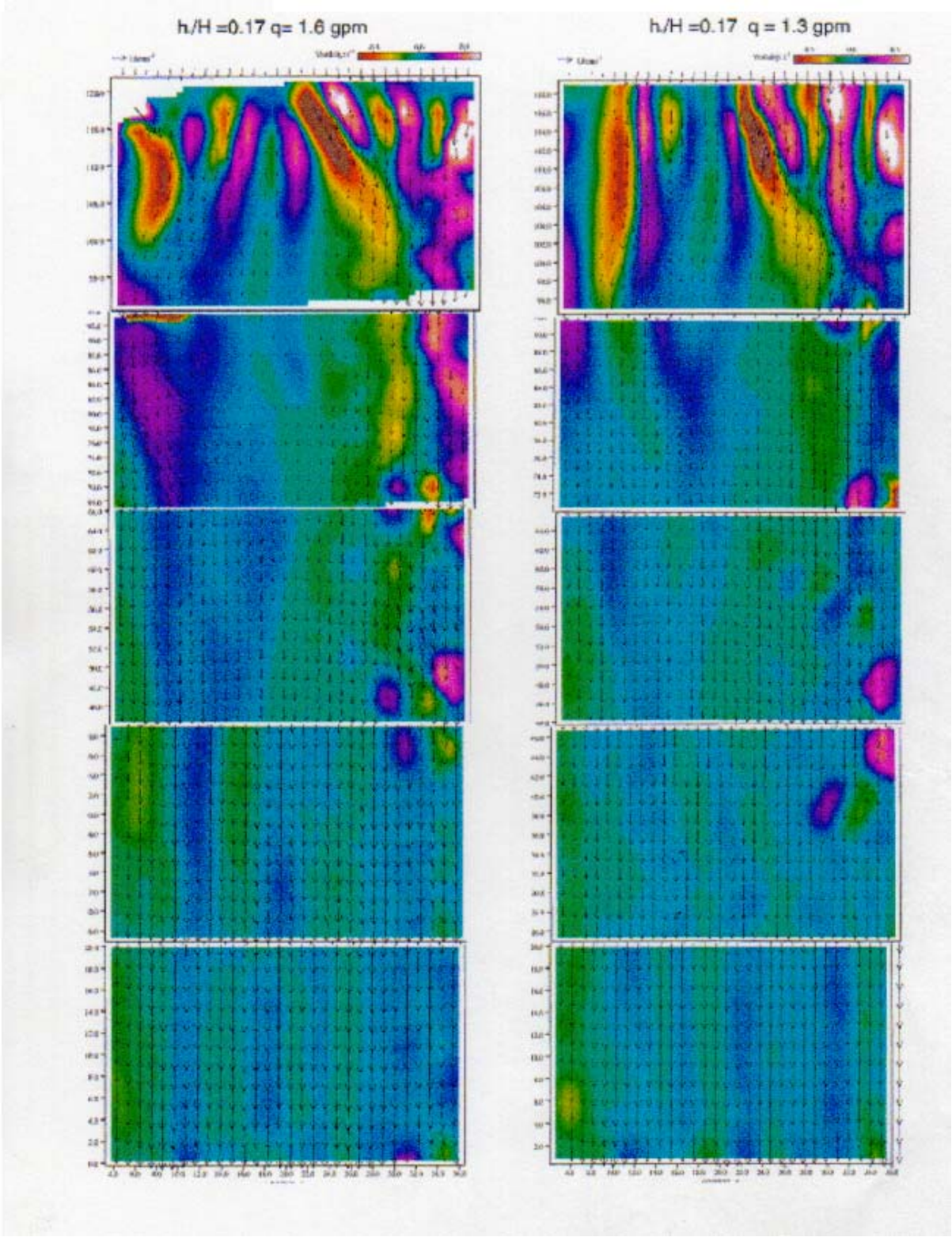

Figure 14. - Top view of deep zone. S = 35 percent and θ = 20 degrees.

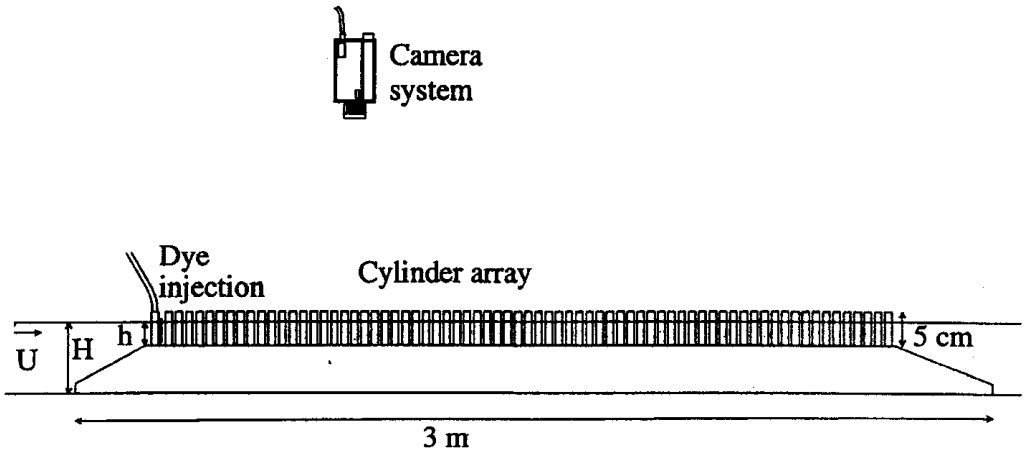

Figure 15. – Experimental setup for measuring concentration.

The mean was then fitted with a Gaussian concentration distribution, C, of the form

$$C = C_o \exp[-U(r-x)/(2\kappa t)] \qquad (15)$$

Where C_o is the concentration of dye at y = 0. U is the mean flow velocity along the x-axis, $r^2 = x^2 + y^2$ to evaluate the lateral diffusion coefficient. Figure 16 shows typical instantaneous, averaged, and fitted Gaussian curves for the concentration distribution of a particular experiment. It displays normalized dye concentration profiles of an instantaneous frame (dots), a mean over 2 minute frames (solid line) and the Gaussian profile predicted from equation 15 (dashed line) used for determining the dispersion coefficient. This case corresponds to an experiment carried out at 20 percent solid distribution, h = 3.4 cm and Re = 32.

The lateral eddy diffusivities so obtained are plotted in figure 17 for a specific set of conditions as indicated in the figure caption.

The data were normalized according to equation 6 and are presented in figure 18, together with the data reported by Nepf, Sullivan and Zavistoski (1997, Limnology and Oceanography, 42, 1735-1745). In general, the model seems to agree with the data obtained from Nepf et al. (1997), except for a few data points obtained at low Reynolds numbers. In the future design of wetlands, figure 18 can be used to estimate diffusivities in shallow zones.

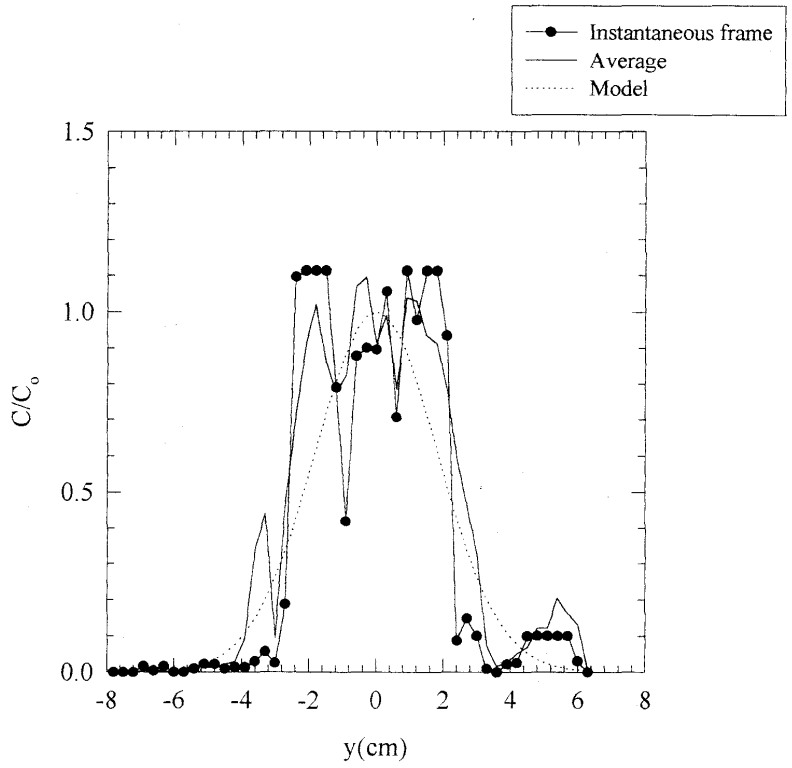

Figure 16. - Normalized dye concentration profiles.

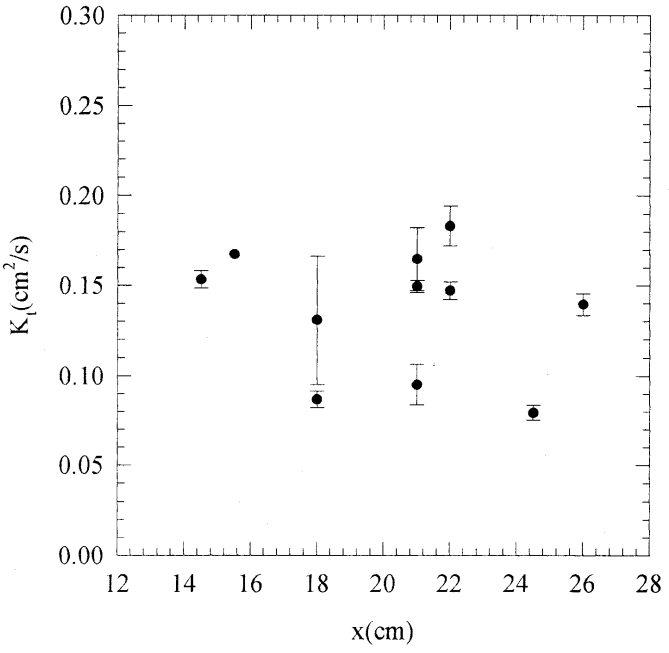

Figure 17. - Lateral dispersion coefficient found at different x-positions along the channel and for the same experimental conditions of Re = 30, h= 3.4 cm, and 35 percent solid plant distribution.

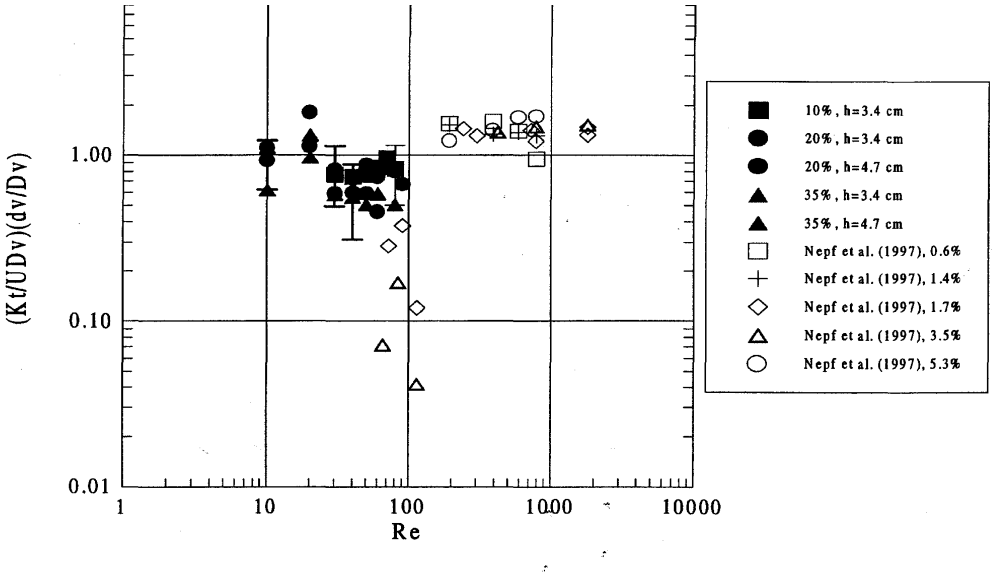

Figure 18. - Theoretical vs. experimental product of the non-dimensional lateral eddy diffusivity and the geometrical factor (dV/DV) against the Reynolds number. Solid symbols correspond to ASU experiments.

FIELD SITE RESULTS AND DISCUSSION

Tracer data was analyzed by the methodology developed by Kadlec for wetlands (Kadlec, 1994). The model framework as proposed by Kadlec (Kadlec, 1996) is a completely mixed tanks-in-series (TIS) concept which accounts for the water mass balance effects due to losses from evapotranspiration and infiltration, and gains from precipitation. Using both the water and tracer mass balance equations, moment equations can be derived which are equivalent to those presented in the literature which do not account for the water mass balance effects. Using linear operator theory for a step input (LaPlace Transforms), the results as developed by Kadlec are:

$$M_{o,N} = \int_0^\infty C_N(t)dt = W/Q_o \sum_{j=1}^{N} a_j \qquad (16)$$

$$M_{1,N} / M_{o,N} = 1/ M_{o,N} \int_0^\infty tC_N(t)dt = \tau \qquad (17)$$

$$M_{2c,N} / M_{o,N} = 1/ M_{o,N} \int_0^\infty (t-\tau)^2 C_N(t)dt = \sigma^2 = \tau^2 \sum_{j=1}^{N} \tau_j^2 \qquad (18)$$

where

$M_{n,N}$ = the n^{th} moment of the exit concentration distribution.

$C_N(t)$ = the exit tracer concentration as a function of time (t).

a_j = water mass balance correction for gains and losses to the system.

N = total number of units in the TIS model.

τ = mean tracer detention time.

τ_j = individual unit detention time.

For tracer testing, the first three moments are of interest. $M_{o,N}$ is a measure of the tracer recovered, $M_{1,N}$ is a measure of the detention time, and $M_{2c,N}$ is a measure of the number of units. Equation (16) shows that the area under the exit concentration curve is not always equal to the amount of tracer added divided by the inlet flow; rather, it is scaled upward if there are evaporative losses, or downward if there is rainfall. Equation (17) indicates that the mean tracer detention time (τ) is the ratio of $M_{1,N}$ / $M_{0,N}$, which is the same result if there were not significant losses or gains from the system under investigation. Equation (18) provides a means for determining the appropriate number of units for the TIS model. Given the measures of σ^2 and τ from the experimental data, a dimensionless variance may be calculated as

$$\sigma^2_\theta = \sigma^2/\tau^2 = \sum_{j=1}^{N} \tau_j^2 \qquad (19)$$

The tracer tests that were successfully completed are presented in table 11.

Table 11. - Tracer test operating conditions

Test	Emergent area depth	HLR (cm/d)	Duration (days)
H1A	1.0 ft	15	9
H1B	1.5 ft	15	12
H1D	1.0 ft	15	11
H2A	1.0 ft	15	9
H2B	1.5 ft	15	11
C1A	1.5 ft	25	13
C2A	1.5 ft	15	13
H2B	1.5 ft	15	11

For all tests, reagent grade NaBr was dissolved in approximately 227 (60 gallons) of source water by stirring with paddles for a minimum of 30 minutes. The NaBr solution was then added immediately downstream of the inlet weir structure. Total time for the slug addition was less than 5 minutes. The exit concentration curve was obtained by

sampling 1 liter of wetland effluent every hour for the test duration, which was defined as 3 times the nominal hydraulic retention time (V/Q_{inlet}) where V is the calculated volume (table 2).

Samples were then analyzed for Br- using either Ion Chromatography (IC) or an ion selective electrode (ISE). Tracer tests H1A and H1B used the IC method, while tests H2A and H2B utilized the ISE. The recovery of tracer using these methods was reasonable (table 12). With the exception of C1A, recoveries ranged from a low of 51 percent to a high of 105 percent. The low recovery from C1A does not include the effect of infiltrating water and approximately 70 percent of the influent water infiltrated during the test consistent with a 24.2 percent recovery.

Table 12. - Hayfield site tracer recovery

Test	% Br- Recovery	Analytical method
H1A	105.3	IC
H1B	50.9	ISE
H1D	91.4	IC
H2A	83.9	IC
H2B	97.9	ISE
C1A	24.2	IC
C2A	83.9	IC

The tracer exit concentration curves for tests H1A, H1B, H2A, and H2B are shown in figure 19. All tests were conducted under an HLR of 15 cm/d, and under either a 1.0- or 1.5-foot emergent area depth. The TIS numerical analysis of the moments is provided in table 13.

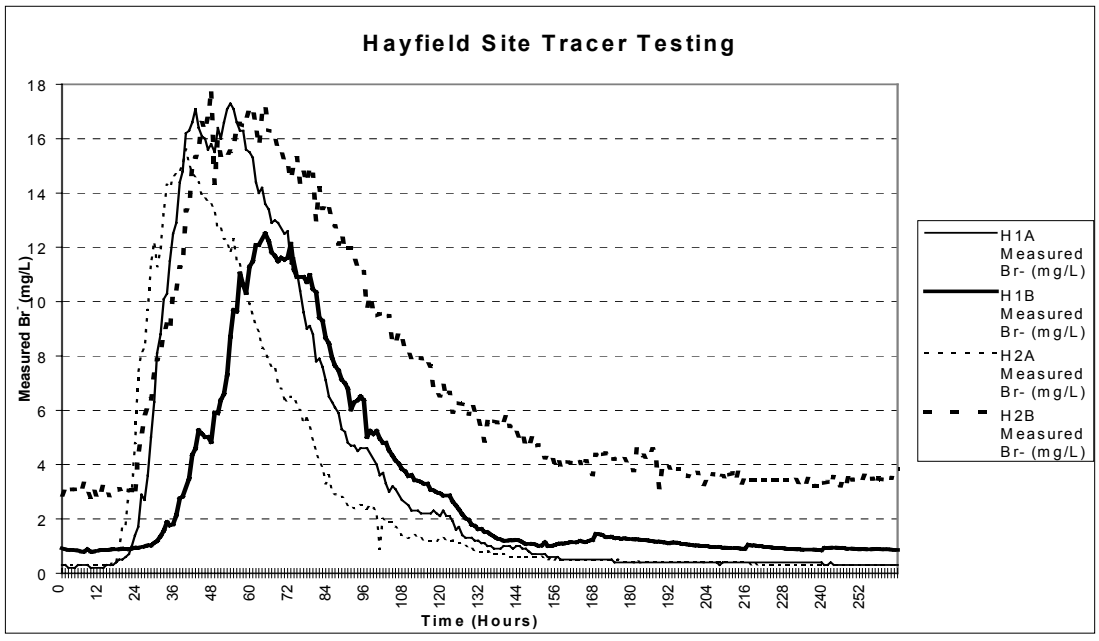

Figure 19. - Tracer exit concentration curves for tests H1A, H1B, H2A, and H2B.

Table 13. - Summary of the moment analyses for the Hayfield site tracer tests

Parameter	H1A	H1B	H2A	H2B
Nominal τ (d)	2.70	3.37	2.34	3.48
As-built τ_o (d)	3.47	4.77	3.13	4.29
Inferred τ_o (d)	2.50	3.16	2.13	3.17
Dispersion number, D	0.11	0.09	0.14	0.16
No. of tanks N	5	6	4	3
No. of deep zones	5	5	2	2
Depth (ft)	1	1.5	1	1.5

The As-built τ_o represents the calculated detention time of the empty basins as constructed without plants. Note that all these tests were performed with dense vegetation during similar time periods. The Nominal τ is the detention time calculated from the tracer tests without considering the effects of evapotranspiration, precipitation, and infiltration. The Inferred τ_o is the detention time calculated from the tracer tests correcting for all effects on the water balance. Considering basin H1, an increase in depth of 0.5 feet resulted in increased detention, but a decrease in dispersion. At the 1-foot depth, basin H1 could be modeled as 5 TIS, and increasing the depth resulted in 6 TIS. Interestingly, the trend seen in H1 was opposite of that in basin H2, which only possesses two deep zones. Although the tracer detention time increased with depth in H2, as was seen in H1, the dispersion number also increased, which was opposite of what occurred in H1. Also opposite was a reduction in the number of TIS when the depth was decreased from 4 feet to 3 feet.

When considering differences between the two basin deep zone configurations and tracer responses, it would appear that the multiple narrow deep zone configuration produces hydraulics which are more "plug-flow" than a basin with two large deep zones. The five deep zones also seemed less sensitive to a change in depth with respect to tracer detention time and dispersion number.

The tracer exit concentration curves for tests H1D, C1A and C2A are shown in figures 20, 21, and 22, respectively. The H1D test was conducted under an HLR of 15 cm/d, and a 1.0-foot emergent area depth. In comparison to H1A and H1B, there was negligible vegetation present during H1D. The CIA test was conducted under an HLR of 25 cm/d, and a 1.5-foot emergent area depth. The C2A test was conducted under an HLR of 15 m/d, and a 1.5-foot emergent area depth.

The TIS numerical analysis of the moments is provided in table 14.

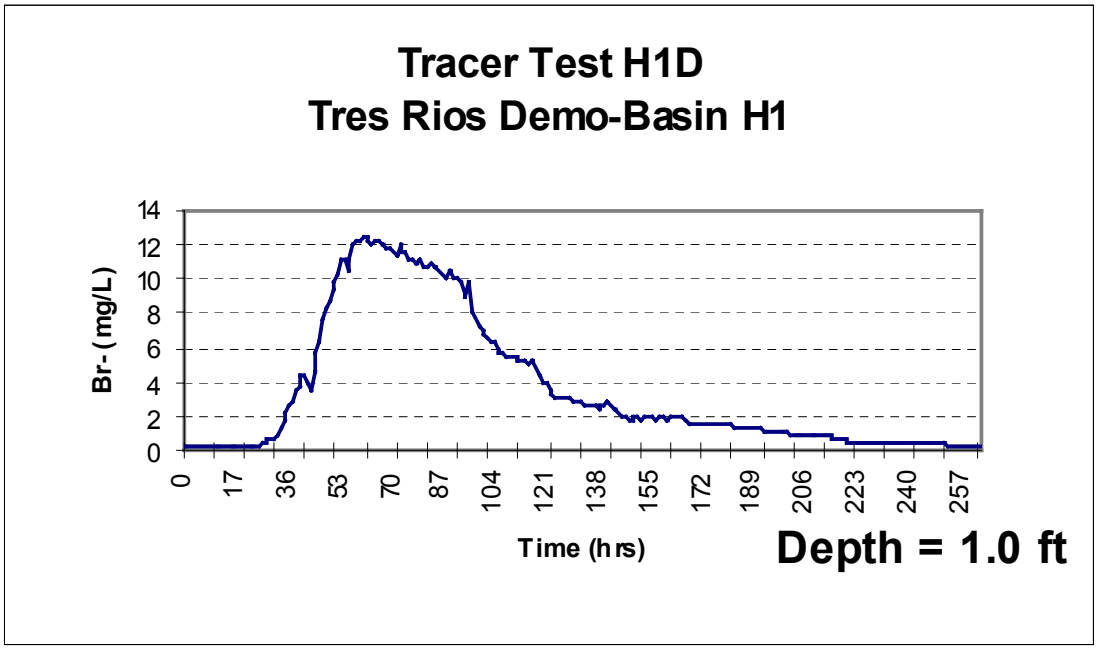

Figure 20. - Tracer exit concentration curves for test H1D.

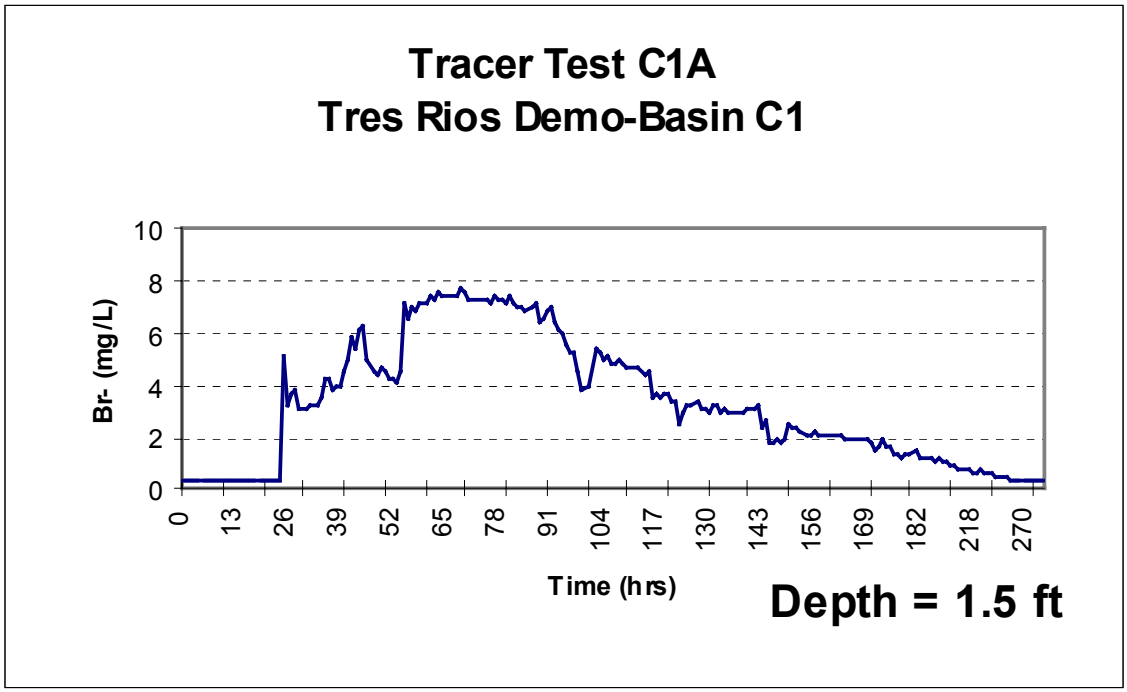

Figure 21. - Tracer exit concentration curves for test C1A.

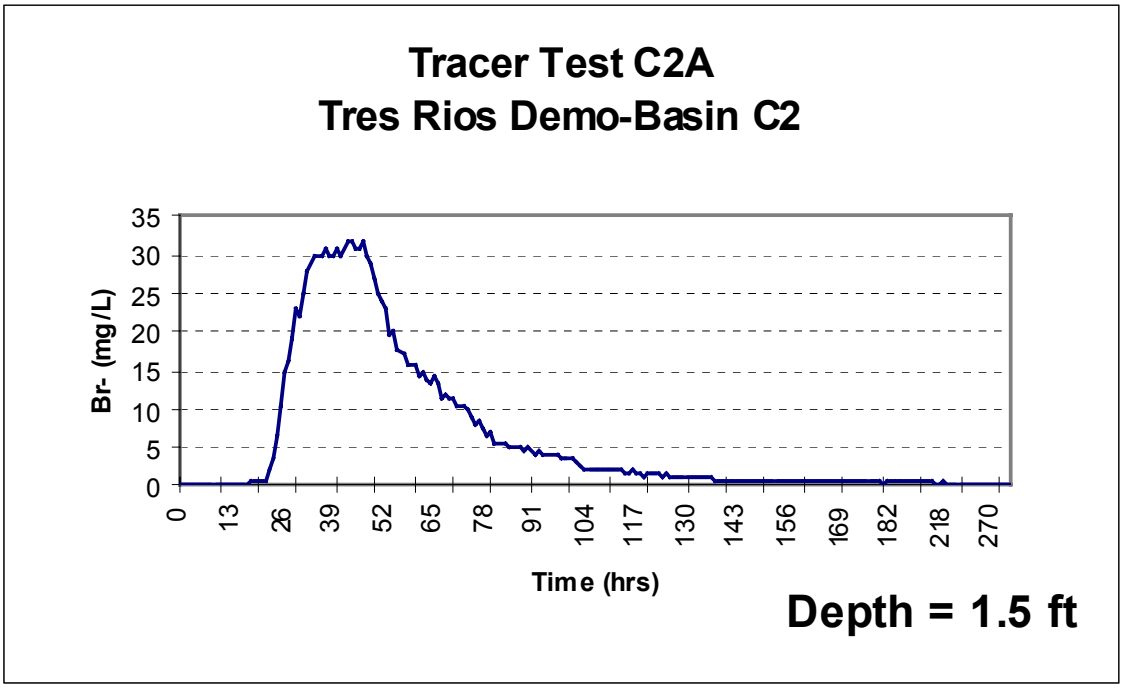

Figure 22. - Tracer exit concentration curves for test C2A.

Table 14. – Summary of the moment analyses for tests H1D, C1A, and C2A

Parameter	H1D	C1A	C2A
Nominal τ (d)	3.56	4.7	3.34
As-built τ_o (d)	3.56	2.95	3.34
Inferred τ_o (d)	3.48	2.38	1.84
Dispersion number $\mathcal{D}$	0.12	0.15	0.22
No. of tanks N	5	4	3
No. of deep zones	5	3	3
Depth (ft)	1	1.5	1.5

It is of interest to compare the results from tests H1A and H1D. These tests were performed at identical depths and hydraulic loadings. The difference between the tests is that there was dense vegetation during test H1A, while there was negligible vegetation during test H1D (figures 23-25). Note that for test H1D, the nominal τ is the same as the As-built τ_o since there was negligible vegetation. Also, the Inferred τ_o is very similar to the Nominal τ indicating that the tracer test results were consistent with a wetland basin with negligible vegetation during a time period when there is negligible evaporation. For test H1A, the As-built τ_o is significantly greater than the Nominal τ as a consequence of vegetation occupying a significant volume in the emergent zone (approximately 50 percent of the volume).

Figure 23. - Dense vegetation in basin H1 representative of conditions during test H1A.

Figure 24. - Dead vegetation in basin H1.

Figure 25. - Sparse vegetation representative of conditions during test H1D.

In comparing the Dispersion numbers for H1A and H1D, we see they are almost identical. Also, the predicted number of tanks is identical for both H1A and H1D. From these results, it appears that the deep zones dominate the macroscopic flow characteristics of basin H1. During tests H1A and H1D, the five deep zones were identical, while the vegetative zones were very different, yet the tracer curves were almost identical in dispersion and number of tanks.

Test C1A was unique in that a high hydraulic loading was used and basin C1 had a high infiltration rate. The curve has a long tail as a result of infiltration slowing down the horizontal velocity of water. One would expect a higher velocity of water near basin C1 inlet and the velocity will decrease near basin C1 effluent since the majority of the influent water infiltrates by vertical movement. Consequently, the nominal τ is much greater than the As-built τ_o. After correction for infiltration, the Inferred τ_o is similar to the As-built τ_o. Basin C1 is unique and is not generally representative of most wetland systems.

Test C2A is not directly comparable to tests as the Hayfield site or to Test C1A. Basin C2 is lined to minimize infiltration and basin C2 was modified for mosquito control, so its deep zone design was changed dramatically as compared to basins H1 and H2. It should be noted that the number of tanks in series derived from analysis of tests C1A and C2A are similar to the number of deep zones.

COMPARISON OF FIELD-SCALE TRACER STUDIES AND PHYSICAL MODELING

The physical model studies predicted a regime for establishment of recirculation in deep zones as a function of flow rate (Re_H) and water depth (h_o/H). During field-scale tracer studies, the Reynolds number is a function of the hydraulic loading and the water depth. During the majority of field-scale studies, the hydraulic loading was constant while the water depth was varied. As the water depth decreases, the Reynolds number increases. Figure 13 (page 30) predicts that for the range of hydraulic loadings (0.8 gpm to 1.8 gpm) studied during field tests, the deep zones will have established recirculating zones. This implies that there will be complete mixing in the deep zones. Field-scale tracer tests on basin H1 consistently had the number of stirred tanks equal to 5 or 6, and basin H1 had 5 deep zones. Each deep zone appeared to behave as a completely mixed system. It is also interesting to note that the result was the same with and without vegetation in the emergent zones. The recirculation patterns predicted by the laboratory studies appear to dominate the macroscopic flow patterns observed in basin H1.

In general, the number of mixed tanks in series derived from analysis of the field-scale tracer studies was similar to the number of deep zones. Basin H2 had two deep zones, and analysis of the tracer studies resulted in three mixed tanks in series at a depth of 1.0 feet and four mixed tanks in series at a depth of 1.5 feet. At a depth of 1.0 feet, the Reynolds number is greater than at a depth of 1.5 feet. However, for both depths, the physical model predicts that recirculation zones should be established in the deep zones. In comparing results from basin H1 and H2, one must wonder why the number of mixed tanks in series was greater than the number of deep zones for tests H2A and H2B. Both the deep zones and the emergent zones in basin H2 are more than twice as long as the zones in basin H1. The effect of increased deep zone depth should not be important since recirculation is established above the slope during the transition from the emergent zone to the deep zone. After a horizontal distance of approximately L = 2H (figure 2b) in the deep zone, the flow field becomes evenly distributed during physical model simulations and no additional recirculation is observed. It is possible that environmental factors such as wind influence field-scale results; however, the establishment of additional recirculation in the deep zones from environmental factors seems unlikely. Another explanation is from the increased length of the emergent zones in basin H2 as compared to basin H1. One effect of the increased emergent zone distance is a significantly greater dispersion number from tests H2A and H2B as compared to H1A and H1B. The greater number of deep zones in basin H1 cause the flow field to redistribute before entry into an emergent zone a greater number of times as compared to basin H2. In basin H2, there are increased opportunities for flow to follow a path of least resistance in an emergent zone and then redistribute by lateral dispersion. Such an effect would increase the apparent number of mixed tanks. A channel dug by a beaver was observed in one of the vegetative zones that could clearly result in a path of least resistance. It is interesting to note that the dispersion number increases as the depth increases in basin H2, while the number of mixed tanks in series decreases as the depth increases. The increase in depth from 1.0 feet to 1.5 feet theoretically increases the residence time in the vegetative zone by 50

percent, while the increase in deep zone residence time is only 11 percent. The increased residence time in the vegetative zone would logically increase the dispersion number.

Relating the lateral eddy diffusivity from analysis at a microscale to longitudinal dispersion from full-scale tracer studies is difficult. The studies of lateral eddy diffusivity did demonstrate how channeling can develop in full-scale systems and how lateral diffusion will occur. The theoretical relationship developed in figure 13 (page 30) demonstrates that lateral diffusivity is a function of velocity, emergent vegetation diameter, and distance between plants. The disconnect between lateral eddy diffusivity and longitudinal dispersion is most apparent when considering tests H1A and H1D. The dispersion numbers are similar for both tests even though H1A had dense vegetation, while negligible vegetation was present during H1D. These results would suggest that the deep zones dominated longitudinal dispersion in basin H1 and the effects of lateral diffusivity were not important.

For tests C1A and C2A, higher dispersion numbers were observed as compared to tests in basin H1. Both basins C1 and C2 had vegetative zone lengths similar to basin H2 and were, therefore, more than twice as long as basin H1. The increased vegetative zone length increased the dispersion number for tests C1A and C2A. However, unlike results from basin H2, the number of mixed tanks in series from tests C1A and C2A was consistent with the number of deep zones. If these differences are the effects of lateral diffusivity in the emergent zones, then the variable distribution of plants must influence the impact on longitudinal dispersion and the number of mixed tanks.

CONCLUSIONS

- A physical model of a full-scale wetlands was constructed at a scale of 20:1. Examination of flow fields in the model provided insight into micro-scale flow characteristics of full-scale wetlands.

- Recirculation zones are established above the slope during transition from the emergent zone to the deep zone. The Reynolds number and the ratio of the emergent zone depth to the deep zone depth (h_o/H) and the slope are important factors. Generally speaking, as the Reynolds number increases, recirculating patterns increase. As the slope decreases, lower Reynolds numbers are required to establish recirculation.

- The relationship between slope and deep zone depth for the establishment of recirculation can be predicted by equation 14 (page 27), reproduced below:

$$H = \gamma\left(\alpha^2 h_o\right)^3 \sqrt{\frac{\alpha r_o^{\,2} U_o}{2 h_o \nu}}$$

- The deep zone length is not critical to establish recirculation.

- The full-scale wetlands used in this study were operated at hydraulic loadings significantly greater than other wetlands. At lower hydraulic loadings, the Reynolds numbers might not be sufficient to establish recirculation. Equation 14 should be used to assess the design of deep zones to ensure recirculation is established.

- Lateral diffusivity does not appear to affect longitudinal dispersion. Longitudinal dispersion does appear to increase as vegetative zone decreases.

- The lateral diffusivity can be estimated by theory. Excellent agreement between theory and experiment was observed (figure 18).

- The full-scale wetlands tracer test analysis yielded a number of mixed tanks similar to the number of deep zones. The conditions under which the tests were performed should have established recirculation in the deep zones, making each deep zone behave as a completely mixed system. Some tests had a number of mixed tanks greater than the number of deep zones; however, the number of mixed tanks was never less than the number of deep zones.

REFERENCES

Al-A'ama, M.S. and G.F. Nakhla, 1995. Wastewater Reuse in Jabail, Saudi Arabia, *Water Research*, 29: 1579-1584.

Brutsaert, W. 1993. Horton Pipe Hydraulics and the Atmospheric Boundary Layer. *Bull. Air Soc.* 74: 1131-1139.

Cisneo, R. 1985. Modeling windfields and surface layer wind profiles over complex terrain and within vegetative canopies. *The Forest-Atmosphere Interactions* (Eds. B.A. Hutchinson and B.B. Hicks, Reidel Co.): 501-520.

Clifford, D. and X. Liu, 1993. Biological denitrification of spent regenerant brine using a sequencing batch reactor. *Water Research*, 27(9): 1477-1484.

Crother-Christie Moon, M. 1994. Reclaiming Water with Wetlands, *Civil Engineering*, 64(7): 52-55.

Goldstein, S. 1965. *Modern Developments in Fluid Mechanics*, Wakes; Dover Publications, NY, 2(3): 548-600.

Kadlec, R.H. 1994. Detention and mixing in free water wetlands. *Ecol. Eng.*, 3(4): 1-136.

Kadlec, R.H. 1996. Interpretation of Tracer Tests for Leaky Treatment Wetlands – The Tanks-in Series Model. Unpublished work from Tres Rios Demonstration Project, Phoenix, AZ.

Kadlec. R.H. and R.L. Knight. 1996. Treatment Wetlands, Lewis Publishers, Boca Raton.

Machate, T., Noll, H., and H. Behrens, 1997. Degradation of phenanthrene and hydraulic characteristics in a constructed wetlands. *Water Research*, 31(3): 554-560.

Littlejohn, D., and S.C. Chang, 1984. Identification of species in a wet flue gas desulfurization and denitrification system by Laser-Raman Spectroscopy. *Environmental Science and Technology*, 18: 305-310.

Martin, J.P., Girts, M.A. and F.J. Koncewicz 1995. Natural system for combined treatment of mine tailings and industrial landfill leachates, *Iron and Steel Engineer*, 72(6): 33-36.

Mitsch, W. J. and J. G. Gosselink, 1993. Wetlands, Von Nostrand Reinhold, New York.

Stark, L.R., Williams, F.M., and W. Wenerof, 1996. The effects of substrate type, surface water depth, and flow rate on manganese retention in mesocosm wetlands, *Journal of Environmental Quality*, 25(1): 97-106.

Wass, R., 2001. Status Report to the 1998 Research Plan for the Tres Rios Demonstration Constructed Wetland Project. Wass-Gerke and Associates, Inc., Phoenix, AZ.

Yang, P.Y., Nitisoravat, S., and J.S. Wu, 1995. Nitrate using a mixed-culture entrapped microbial cell immobilization process under high salt conditions. *Water Research* 26(6): 1525-1532.